Analysis of Turbulent Properties in the Near Field of an Isothermal Free Jet

by

Luai M. Al-Hamas Al-Hadhrami

A Thesis Presented to the

FACULTY OF THE COLLEGE OF GRADUATE STUDIES

KING FAHD UNIVERSITY OF PETROLEUM & MINERALS

DHAHRAN, SAUDI ARABIA

In Partial Fulfillment of the
Requirements for the Degree of

MASTER OF SCIENCE

In

MECHANICAL ENGINEERING

December, 1996

INFORMATION TO USERS

This manuscript has been reproduced from the microfilm master. UMI films the text directly from the original or copy submitted. Thus, some thesis and dissertation copies are in typewriter face, while others may be from any type of computer printer.

The quality of this reproduction is dependent upon the quality of the copy submitted. Broken or indistinct print, colored or poor quality illustrations and photographs, print bleedthrough, substandard margins, and improper alignment can adversely affect reproduction.

In the unlikely event that the author did not send UMI a complete manuscript and there are missing pages, these will be noted. Also, if unauthorized copyright material had to be removed, a note will indicate the deletion.

Oversize materials (e.g., maps, drawings, charts) are reproduced by sectioning the original, beginning at the upper left-hand corner and continuing from left to right in equal sections with small overlaps. Each original is also photographed in one exposure and is included in reduced form at the back of the book.

Photographs included in the original manuscript have been reproduced xerographically in this copy. Higher quality 6" x 9" black and white photographic prints are available for any photographs or illustrations appearing in this copy for an additional charge. Contact UMI directly to order.

UMI

A Bell & Howell Information Company
300 North Zeeb Road, Ann Arbor MI 48106-1346 USA
313/761-4700 800/521-0600

Analysis of Turbulent Transport Properties in the Near Field of an Isothermal Free Jet

Luai M. Al-Hamas Al-Hadhrami

Mechanical Engineering

December 1996

KING FAHD UNIVERSITY OF PETROLEUM AND MINERALS

DHAHRAN, SAUDI ARABIA

COLLEGE OF GRADUATE STUDIES

This thesis, written by **Luai M. A. Al-Hammas Al-Hadhrami** under the direction of his Thesis Advisor and approved by his Thesis Committee, has been presented to and accepted by the Dean of the College of Graduate Studies, in partial fulfillment of the requirements for the degree of **MASTER OF SCIENCE** in **MECHANICAL ENGINEERING**.

THESIS COMMITTEE

Saad Ahmed
Dr. Saad A. Ahmed (Chairman)

Dr. Bekir S. Yilbas (Member)

Dr. Ahmet Z. Sahin (Member)

Dr. Syed A. Said (Member)

Department Chairman Dr. Muhammed O. Budair

Dean, College of Graduate Studies Dr. Abdallah Al – Shehri

18-5-97
Date

كلية الدراسات العليا
COLLEGE OF GRADUATE STUDIES

ACKNOWLEDGEMENTS

In the name of Allah. Most Gracious. Most Merciful

"Read in the name of thy Lord and Cherisher. who created. Created man from a [leech-like] clot. Read and thy Lord is Most Bountiful. He Who taught [the use] of the pen. Taught man that which he knew not. Nay. but man doth transgress all bounds. In that he looketh upon himself as self-sufficient. Verily. to thy Lord is the return [of all]" (The Holy Quran. Surah 96

All praise and glory be to Almighty Allah who gave me courage and patience to carry out this work. and peace and blessings of Allah be upon Prophet Muhammad. Acknowledge is due to King Fahd University of Petroleum and Minerals for providing support for this research.

My deep appreciation goes to my advisor Dr. Saad A. Ahmed. for his constant help. guidance and the countless hours of attention he devoted throughout the course of this work. He was always kind. understanding and sympathetic to me.

Thanks are also due to my thesis committee members Dr. Bekir S. Yilbas, Dr. Ahmet Z. Sahin and Dr. Sayed A. Said, for their interest, cooperation, advice and constructive criticism.

Special thanks are due to my colleagues and friends for their help and encouragement. They have made my stay at KFUPM a very pleasant and unforgettable experience.

Finally, my heartfelt thanks and gratefulness to my parents and other family members for their encouragement and moral support.

Contents

List of Figures

List of Tables

THESIS ABSTRACT

Name: Loai Al - Hadhrami

Title: Analysis of Turbulent Transport Properties in the Near Field of an Isothermal Turbulent Free Jet

Degree: Master of Science

Major Field: Mechanical Engineering

Date of Degree: December 1996

Simultaenous two-component laser Doppler velocity measurements were made in the isothermal, turbulent flowfield, of an axisymmetric jet. Mean velocities, normal and shear stresses and triple products were measured, and presented at axial positions $\frac{x}{D} = 1$ *to* 22. *A balance of turbulent kinetic energy in the flow was performed. The production, convection and diffusion of turbulent kinetic energy were computed directly from the experimental data using central differences. In this study, three velocity bias correction schemes were used and the effects of each of them on the behavior of the mean velocities, normal and shear stresses, triple products, production terms, convection terms and diffusion of the turbulent kinetic energy will be presented.*

Keywords: Turbulent flow, Free jet, Turbulent kinetic energy.

Master of Science Degree
King Fahd University of Petroleum and Minerals, Dhahran.
December 1996

ملخص الرسالة

الاسم	:	لؤي بن محمد بن علي الهمس الحضرمي
موضوع الرسالة	:	قياس السرعات الدوامية المصاحبة لاندفاع الهواء لنفاث متماثل
التخصص	:	هندسة ميكانيكية
التاريخ	:	ديسمبر ١٩٩٦

في هذه الأطروحة استخدم جهاز ليزر مركب من عنصرين لقياس السرعات الدوامية المصاحبة لاندفاع الهواء لنفاث متماثل . وقد تم قياس السرعات المختلفة بالاضافة الى الاجهادات القصية والسرعات الثلاثية في مواقع مختلفة تبدأ من ١ حتى ٢٢ قطر النفاث .

لقد تم أيضا دراسة الطاقة المصاحبة للحركة الدوامية من حيث انتشارها وانتقالها وتبديدها مستخدمين برامج متطورة خاصة بالحركة الدوامية . وقد استخدمت ثلاث طرق حسابية مختلفة في تحليل القياسات ولقد درس تأثير كل من هذه الطرق على نتائج السرعات المتوسطة وعلى الطاقة المصاحبة للحركة الدوامية من حيث انتشارها وانتقالها وتبديدها .

درجة الماجستير

قسم الهندسة الميكانيكية

جامعة الملك فهد للبترول والمعادن

الظهران – المملكة العربية السعودية

ديسمبر ١٩٩٦

Chapter 1

INTRODUCTION

1.1 Review of Turbulent Jet Measurements

Turbulent free jets have been studied by several researchers partly because of their numerous practical applications and their relative simplicity and universality. They provide very simple and good test cases for the developers of turbulence models. Their flowfields are usually considered to contain the following three zones: a) the far field, b) the transition (or intermediate) field and c) the near field. In the far field, self-similarity is a characteristic of the mean velocity field: and it has been the subject of investigation by many researchers: therefore, its study is not of prime interest in the present investigation. This study is concerned with an experimental investigation of the near and intermediate field of an isothermal free jet. The objective of this program is two fold: First, to establish a basic confidence

level in the laser Doppler velocimeter (LDV) bias correction techniques. Second, to provide additional detailed insight into the flowfield of a free jet. Many investigators have made studies about free jets, such as Corrsin and Uberoi [1] who measured the power spectra of velocity and temperature fluctuations in heated and unheated jets using crossed hot-wire. They concluded, from their measurements of the shear-correlation spectrum, that the fine structure in the shear flow in a round turbulent jet is isotropic.

Single and double hot-wires were used by Kolpin [2] to determine turbulence intensity and shear stress in the mixing region of a round jet. He found that, above a certain Reynolds number, the jet diameter plays no role in the description of the turbulent field and that the generation of turbulence, governed by the interaction of the large eddies and the mean flow, is a local phenomenon. Davies et al. [3] also conducted experiments in the mixing region in which the turbulence intensity, turbulence spectra, and shear stress were measured. Results indicated that the local intensity of the turbulence is equal to 0.2 of the shear velocity.

Measurements in the self-preserving region of a jet were performed by Wygnaski and Fiedler [4] and Rodi [5] using hot-wire probes. The mean velocities, normal stresses and shear stresses measured by Wyghanski ad Fiedler [4] were also obtained by Rodi [5] as a check. Rodi processed the signals from the hot-wire anemometer using two different methods: the conventional method and a new method which determines the fluctuating velocities from the squared electrical signal. The results

agree between the two studies when conventional processing is used but higher values are reported in Rodi's investigation with the squared data processing. Unfortunately, this new method is not applicable to low turbulence intensity flow (i.e.: flows with less than 25% turbulence intensity).

Bradshaw et al. [6] conducted measurements of turbulence properties in the noise producing region of a free round jet. It was found that the flow in this region is dominated by a group of large eddies, containing nearly a quarter of the turbulent shear stress in the quasi-plane region of the shear layer.

Corrsin [1] used a four hot-wire probe to measure the turbulence quantities and a pitot tube to measure the mean velocity in a heated round jet. Mean axial and radial velocities turbulence intensities and turbulent shear stresses were determined by Sami et al. [8] using a single and crossed hot-wire probes in the flow-establishment region of an air jet issuing into still air. Mckillop [9] performed turbulence measurements such as mean velocities, RMS values and shear stress at acertain locations, which are compared to the present study. A recent research was done by Nao et al.[10] by using three-dimensional particle tracking velocimetry (3-D PTV) to measure the instantaneous velocity vectors and detailed distributions of the turbulent statistics of the mean velocities, fourth order correlations and Reynold's stress in the self-preserving region of an axisymmetric free jet.

1.2 Review of Laser Doppler Velocimeter Systems

Conventional instrumentation systems such as hot-wire anemometers and pitot probes, interact with the flow environment and introduce local flow disturbances. The devices are: moreover, subject to damage because of impact and thermal loadings. For either of these systems, it becomes difficult to interpret measurements of the mean velocity in flows having high local turbulence levels (See Goldstein [11] and Hinze [12]). The pitot tube, moreover, does not adequately respond to fluid transients and is insensitive to flow direction (See Gettelman and Krause [13]) so that it is of little use in measurements of turbulence. Hot-wire anemometers, while providing accurate turbulence information, are fragile, and are limited to moderate turbulence levels as reported by Hinze [12] and Bradshaw [14]. They lose sensitivity in high velocity flows (See Pai [15]), and require an independent measurement of fluid temperature in nonisothermal flow situations (see Bradshaw [14], and Jones [16]).

Many of these difficulties are avoided by optical measuring devices such as laser velocimeter. Since the LDV does not materially interact with the flow, it neither creates disturbances nor is subject to damage from the flow environment. Since the first demonstration of this instrument in 1964 by Yeh and Cummins [17], it has undergone extensive development so that many of its early limitations related to optics alignment and the processing of high frequency signals have been solved by Lennert

et al. [18]. In view of the many recent applications of velocimeter to a wide variety of practical flow problems (See Stevenson and Thompson [19], McLaughlin and Tiederman [20], Stevenson and Thompson [21]), it appears that the laser velocimeter is a reliable tool to provide detailed velocity information. For an LDV system, velocities are determined from the rate at which a particle intercepts fringes established in the probe volume. A one component fringe system with crossed-beam input optics (See Lennert et al. [18], Rudd [22]) is shown in Figure 1.1. Light from a highly coherent light source, such as a laser, is split into two equal intensity beams and focused at a point in the flow by a collimating lens. With this optical arrangement, interference fringes are created in the probe volume formed by intersection of the input beams. Particles contained in the fluid medium are swept through the probe volume and scatter light which is focused by collector optics on a photo-detector. A high frequency Doppler burst signal results, which may be analyzed to give the frequency at which a particle intercepts the fringes.

The velocity of an individual particle (V_i) is related to the signal period (τ_i) by the relation

$$V_i = K_V/\tau_i \tag{1.1}$$

Where K_V is the fringe spacing (or calibration constant) defined by

$$K_V = \lambda/2\sin(\theta/2) \tag{1.2}$$

For the depicted case, the wavelength of the incident light (λ) and convergence angle of the beams (θ) are solely determined by the input optics so that the LDV requires no information on the properties of the fluid medium to obtain velocity measurements. The accuracy of the result; however, is dependent on how well the particle velocity represents the fluid velocity at the instant of observation, the accuracy to which the period is determined, and the stability of the fringe system.

When the concentration of particles is sufficiently high (i.e.: at least one particle is found in the probe volume at any time), conventional frequency trackers may be used to determine the mean and root mean square (RMS) values of the Doppler frequency. Such systems may be termed continuous wave LDV's, and the data may be treated in a similar fashion to that from hot-wire anemometers. In gases, however, the particle concentration is generally too low for continuous wave operation unless the flow is artificially seeded. In many cases, seeding is undesirable because of constraints imposed by test equipment and the fact that multiple particle interactions lead to ambiguities (see George and Lumbley [23]), which reduce the accuracy of the results. This has lead to the development of data processors (see Brayton et al. [24]), Asher [25] capable of measuring the period or frequency of individual Doppler bursts so that measurements may be made at the low natural particle concentrations typical of gas flows. Detailed information on the statistical properties of the flow are then obtained by averaging the results of many individual realizations of particle velocity.

For any type of laser velocimeter, a fundamental limitation is that the results may be compromised by particle dynamic effects. It can be shown that the response of particles to fluid transients is related to the physical characteristics of the particle and the temporal history of the flow (see Meak and Jones [26], Berman [27]). Consequently, there has been questions by Khosla and Lederman [28], Yanta [29] whether LDV's may be used to adequately measure turbulence parameters in the rapidly fluctuating transient velocity fields representing turbulent motions.

It is noted (from Equation 1.1) that no information is provided by a conventional LDV on the direction of travel of a particle through the probe volume. This directional ambiguity is important in highly turbulent, pulsating, and recirculating flows where reversals in fluid motion may occur. Several methods have been proposed for measuring flow directionality with an LDV (see Longan [30], Farmer and Hornkohl [31]) by frequency shifting the Doppler signal so that a zero velocity condition corresponds to a non-zero frequency. One method of achieving this effect is to use ultrasonic diffraction cells to both split the input beam and to impart the desired frequency shift. Such laser vector velocimeters (see Farmer and Hornkohl [31] or Bragg-diffracted LDV's) are particularly well-suited for turbulence studies since they may be used in highly turbulent flows without introducing the aliasing phenomenon found in hot-wires or conventional LDV's. Furthermore, the fringes created by a Bragg-diffracted system move relative to the flow so that the particle

crosses more fringes than in conventional LDV's, making it possible to detect the velocity of particles that traverse the probe volume at relatively large angles to the flow direction. Accordingly, the dead zone (see Lennert et al. [18] characteristic of stationary fringe LDV's) is greatly reduced.

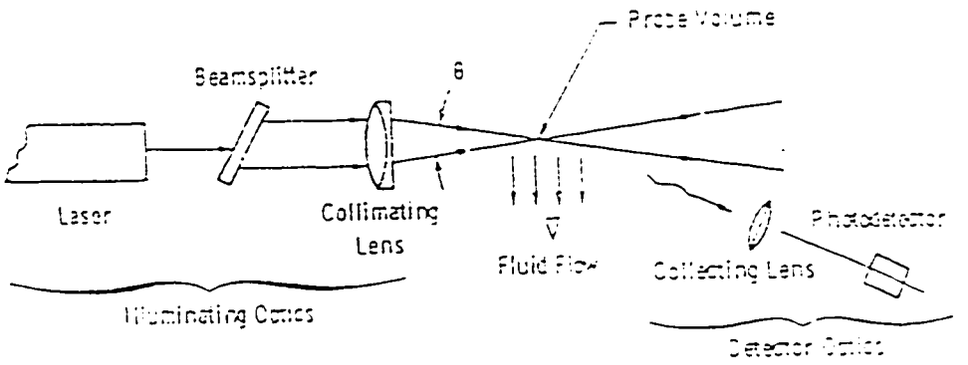

Figure 1.1: Optics for one component LDV system.

1.3 Review of Velocity Bias Associated with LDV Systems

Velocity bias is an error associated with the statistical analysis of the measurements coming from the LDV. For this reason the validity of the LDV data has been questioned. Several types of bias exist due to:

1. The correction between velocity and sampling rate(velocity bias).
2. The ambiguity of the measured flow direction (directional bias).
3. Bias due to density fluctuations.
4. Variation in particle concentrations.
5. Mixing processes.
6. combustion.
7. Electronic imperfection.

The majority of the biasing associated with LDV measurements can be eliminated with the proper choice of optics and shifting of the beams. However, the problem of the velocity bias remains. Analytical prediction of McLaughlin and Tiederman [32] showed the existence of velocity bias. Since then, many investigators have conducted experiments specifically designed to verify the existence of velocity

bias. Others have conducted experiments in highly turbulent flows and employed various correction schemes in their data reduction. Durao and Whitelaw [33] proposed random sampling of the data from burst type processors. Although computer predictions supported their argument, measurements on the center line of a free jet at 25%, 40%, and 100% turbulence intensity levels proved inconclusive. Quigley and Tiederman [34] applied McLaughlin and Tiederman's [31], one dimensional correction scheme to their velocity measurements. The corrected velocities agreed well with the profiles obtained from the pressure drop measurements. Subsequent measurements by Bogard and Tiederman [35] in the same water channel did not agree with the predicted velocity profiles. One of their findings was that particle arrival rate did not affect the velocity measurements. This directly contradicts the findings of Barnett and Bentley [36]. Hoesel and Rodi [37] have proposed a particle separation time correction for non-uniformly seeded flows when the average particle separation is small compared to the time scale of the turbulence. For uniformly seeded flows, they suggest a probe volume residence time correction. They applied their correction scheme to measurements made across a free jet. Near the jet axis, their corrected velocities agreed well with that of McLaughlin and Tiederman's, [31] but deviated toward the edge. Giel and Barnett [38] made LDV and hot-wire measurements in a jet very similar to that of Hoesel and Rodi [36]. They expected an error on the order of 10 %; however, no evidence of velocity bias was found in their study. Johnson, et al. [39] reported measurements in a Mach 2.9 separated bound-

ary layer and in transonic flow past an airfoil. They found no evidence of velocity bias. They claim that velocity bias occur if particle arrival rate is much lower than the turbulence frequencies. This directly contradicts the results of Bogard and Tiederman's experiment. Measurements of Dimotakis et al. [40] of turbulent boundary layer profiles over a flat plate showed that (only after bias correction) LDV and pitot tube measurements did agree well. Criag and Nejad [41] have shown that velocity bias may even occur in flows with low turbulence. This problem usually arises when one is measuring second or third components of the velocity where its mean value is small and the turbulence is nearly isotopic. Simpson and Chew [42] suggested the use of constant time-interval data sampling for elimination of velocity and density biasing. Roesler et al. [43] and Stevens and Thompson [44] have used this technique in their studies. Craig and Nejad [41] further developed this approach and established an easily measurable data collection time interval to indicate when an acceptable ratio of seeding and sampling rates (for constant time-interval data sampling) has been achieved.

A review of the open literature has revealed that unbiased simultaneous, multi-component LDV measurements in turbulent flows are virtually non-existent. In addition to the typical biasing problems, multi-component LDV measurements have the disadvantage of suffering from other types of measurement ambiguities. For example, the fringe patterns of a two-component LDV system are usually not orthogonal; therefore, components of the velocity vector must be resolved from mea-

surements of both Doppler frequencies. Thus, the measurement error in one channel will influence both velocity components. Another matter of concern is the effect of an arbitrarily chosen time interval (coincidence time window) which ensures simultaneous measurements of the velocity components on the measured velocities.

When analyzing velocity bias, three conditions are usually assumed:

1. Uniform seed density.

2. An ellipsoid probe volume.

3. Isotropic conditions existing inside the probe volume

The first condition eliminates the need to consider nonuniform seeding effects from the analysis, while the later two conditions eliminate the need to consider directional dependence.

1.4 Objectives of the Current Work

Although numerous investigators have contributed to the understanding of jet flow as summarized previously in Section 1.1. Knowledge in this areas is still far from complete. Among the shortcomings are the followings:

1. There has been no detailed study of the near jet flowfield for theoretician to employ for comparisons of their computational results to check the validity of numerical models used in the solution.

2. There have been few efforts to relate velocity bias effects to higher order velocity statistics. Given these gaps of knowledge, the objectives of the present study are as follows:

   (a) To define the measurement capability and limitations of the two component LDV system.

   (b) To develop methods for analyzing the velocity measurements and to evaluate bias correction techniques and their limitations.

   (c) To define the jet flow in the near and the intermediate field and also to calculate the kinetic energy terms.

Chapter 2

EXPERIMENTAL FACILITY AND INSTRUMENTATION

2.1 Jet Facility

Figure 2.1 shows a schematic illustration of the isothermal free jet. The nozzle assembly consists of an aluminum settling chamber with two sets of flow straighteners and a contoured discharge section. The nozzle exit diameter is approximately 15.1 mm. The jet exit velocity is kept constant at a nominal value of 30 m/s which gives an approximate Reynolds number of 62000, based on the nozzle exit diameter. The supply air pressure of the jet is regulated to control the volume flow rate through the nozzle. Air temperature is kept approximately the same as the room temperature to ensure an isothermal flow. Titanium dioxide seeds are injected in the settling

chamber far upstream of the nozzle to ensure uniform distribution at the jet exit. Seeds are generated by reaction of titanium tetra-chloride with the water vapor of saturated air in a separate chamber. the design of the seeder and its operational procedure were reported by Craig et al. [45]. The uniform distribution of the seeds at the nozzle exit is checkd by monitoring the data rate across the jet exit to verify if it is approximately constant or not. The jet exit velocity profile of the air is nearly a "top hat" shape, with nozzle exit velocity varying by a maximum of 3% or less of the mean value. The jet tested is assumed to be fully turbulent with turbulence levels of 3% or less, at the exit. To provide a better controlled environment, a large enclosure from plastic sheets is built (1.5 m ×1.5 m). This box is connected in turn with the exhaust system. This type of arrangement helped in prohibiting room drafts from altering the flow, and is used to protect the operator from breathing the contaminated air. It is assumed that this enclosure is large enough not to affect the flow. The nozzle assembly is mounted on a 3-D traversing mechanism which enable precise positioning of the free jet relative to the center of the sampling volume, or the measurements.

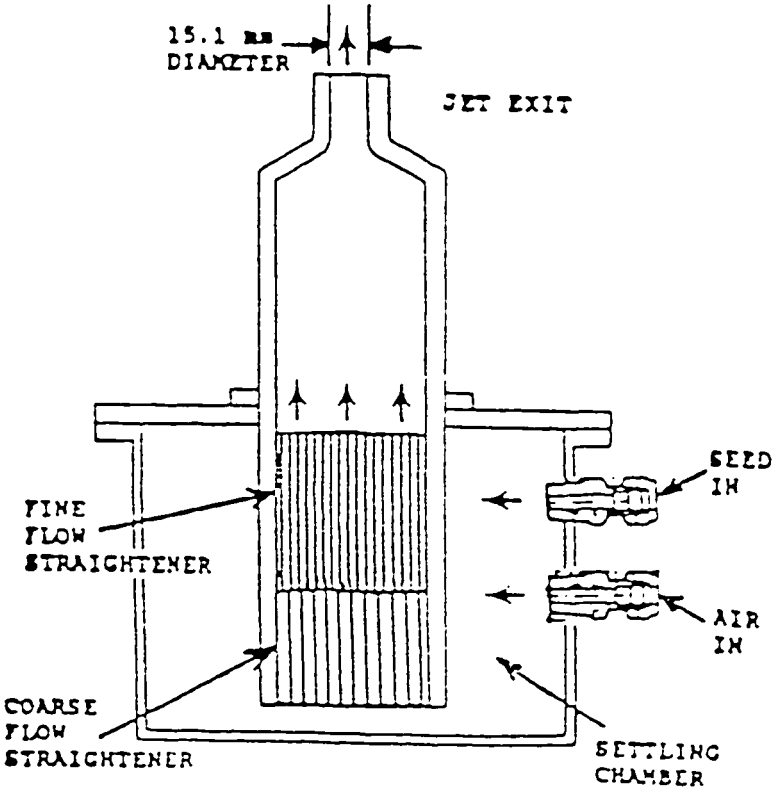

Figure 2.1: Schematic of free jet nozzle assembly.

2.2 Instrumentation and Data Acquisition

A two component LDV system with a four beam configuration is used in the backscatter mode. The system is manufactured by TSI Inc., with several in-house modifications (see Nejad et al. [45]). Two fringe patterns are aligned at a common point in space. These fringes are perpendicular to each other and approximetly 45° to the jet axis. A $20\mu m$ aperture is used in the alignment procedure to ensure that the four beams cross at the same point in air. This arrangement is utilized since the velocity measuerments in both directions will be of the same order of magnitude. Both fringe patterns are frequency shifted 40 MHz using two Bragg cells. The entire optical system is mounted on a 3-D traversing table with a resolution of 0.025 mm (for more details, see reference [47]).

With this arrangement and TiO_2 as the seeding particles (1 micron size approximately), data rates 0f 5000-10000/s are achieved. The corresponding coincidence rates vary between 2000-6000/s when a $20\mu s$ coincidence window (time between two Doppler bursts from two channels) is chosen.

For each measurement location, the upstream flow parameters (i.e.: upstream pressure and temperature, and $\overline{U}_o$) together with the calculated moments and velocity probability density functions (PDF) are displayed on a graphic terminal. A hard copy of these variables is documented and obtained for each radial location.

Three different methods of velocity bias-correction have been examined. First,

the velocity of each particle is measured and the average is calculated directly without any corrections (particle average or biased data denoted "R0N"). The second method involves correcting the previous measurements by utilizing the time between measured data points (T_{bd}) as the weighting function and it is denoted by "R1N". Third, the random digital data from LDV processors are sampled with a constant sampling rate of approximately ≤ 0.1 of the original data rate and is denoted by "CTSN". The details of these techniques were reported earlier by Nejad and Davis [46].

The uncerntainty of the measured main velocities was determined using the techniques described by Snyder et al [48]. The uncertainty $\Delta\overline{U}_o$

$$\Delta\overline{U}_o = 1.96\sigma_u\sqrt{N} \tag{2.1}$$

For 95 % confedence level, the constant 1.96 is used (σ_u is an estimator for the true standard deviation and N is the sample size (minimum N = 4095)). From the above relation, the maximum uncertainty of the main velocity $\overline{U}_o$ due to random errors was found to be 0.3% of the jet exit velocity

2.3 Averaging Schemes

Many sampling and averaging schemes to reduce or eliminate velocity bias have been proposed. Those tested in this investigation are described below.

Particle average : The velocity of each valid particle is measured, and the average

is found arithmetically.

$$\overline{U} = \sum_{i=1}^{N} U_i / N \tag{2.2}$$

As previously discussed, this average may be biased if the particle arrival rate is correlated to U_i, see Table 2.1 for calculating velocity statistics.

T_{bd} average : Barnett and Bentley [36] proposed that the best way to eliminate velocity bias was to start with the definition of the time average.

$$\overline{U} = \frac{1}{T} \int_0^T U(t)\, dt \tag{2.3}$$

and approximate that expression as a sum replacing the differential time, dt, with the time between measured data points, T_{bd}. Thus

$$\overline{U} = \sum_{i=1}^{N} (U_i T_{bd,i}) / \sum_{i=1}^{N} T_{bd,i} \tag{2.4}$$

This method is called the T_{bd} method after the weights assigned to each velocity sample. If the sampling is periodic, the expression reduces to the arithmetic average. The T_{bd} scheme may also be viewed as a correction scheme. (T_{bd} should correct for the bias.(see Reference [35])

Periodic Sampling : Another possible method of eliminating the velocity/data-rate correlation, and therefore the velocity bias, would be to trigger the counter at regular intervals and collect the next Doppler burst to arrive (Stevenson and

Thompson [47]). With this method, the counter analyzes the Doppler bursts at an almost uniform rate f_s which is slower than f_p. Uniform sampling is assumed, and a simple average is used to obtain $\overline{U}_{ps}$. Erdmann and Tropea [50] examined this method farther and also concluded that, if $f_p \gg f_s$, then the velocity calculated using this method would represent an unbiased estimate of $\overline{U}$, while if $f_p \sim f_s$, velocity bias would result.

	Velocity Statistics
General notations	$\overline{U} = \frac{\sum_{j=1}^{N} w_j U_j}{\sum_{j=1}^{N} w_j}$, $\overline{V} = \frac{\sum_{j=1}^{N} w_j V_j}{\sum_{j=1}^{N} w_j}$, $\overline{UV} = \frac{\sum_{j=1}^{N} w_j U_j V_j}{\sum_{j=1}^{N} w_j}$; $\overline{u'^2} = \frac{\sum_{j=1}^{N} w_j u_j'^2}{\sum_{j=1}^{N} w_j}$, $\overline{v'^2} = \frac{\sum_{j=1}^{N} w_j v_j'^2}{\sum_{j=1}^{N} w_j}$
Turbulent velocity fluctuations	$u' = U - \overline{U}$, $v' = V - \overline{V}$
Standard deviation	$\sigma_u = \left[\frac{\sum_{j=1}^{N} w_j u_j'^2}{\sum_{j=1}^{N} w_j}\right]^{1/2}$, $\sigma_v = \left[\frac{\sum_{j=1}^{N} w_j v_j'^2}{\sum_{j=1}^{N} w_j}\right]^{1/2}$
Skewness	$S_u = \frac{\sum_{j=1}^{N} w_j u_j'^3}{\sigma_u^3 \sum_{j=1}^{N} w_j}$, $S_v = \frac{\sum_{j=1}^{N} w_j v_j'^3}{\sigma_v^3 \sum_{j=1}^{N} w_j}$
Flatness	$F_u = \frac{\sum_{j=1}^{N} w_j u'^4}{\left(\sigma_u^4 \cdot \sum_{j=1}^{N} w_j\right)}$, $F_v = \frac{\sum_{j=1}^{N} w_j v'^4}{\left(\sigma_v^4 \cdot \sum_{j=1}^{N} w_j\right)}$
Reynolds shear stress	$\overline{u'v'} = \overline{UV} - \overline{U} \cdot \overline{V}$
Correlation coefficient	$\frac{\overline{u'v'}}{(\sigma_u \cdot \sigma_v)}$

$w_j = 1$ for particle average scheme.
$w_j = T_{bd}$ for T_{bd} average.
$w_j = 1/f_s$ for constant periodic sampling

Table 2.1: Velocity Statistics.

Chapter 3

COMPARISONS BETWEEN LDV AND HOT WIRE RESULTS

Figures 3.1 through 3.5 show comparisons between LDV and hot-wire data of McKillop [9] at axial locations of x/D = 1, 6, 10 and 20. The axial mean velocity measured by the LDV is approximately equal to their respective hot wire values. The differences are small and within the experimental uncertainty of both instruments. In general, the comparisons between LDV and hot wire results shown in Figure 3.1 are satisfactory. However, differences are noted in Figure 3.2 and in the measurements of $\overline{V}/\overline{U}_{cl}$ which are presented in Figure 3.3 and also $\sqrt{\overline{v'^2}}/\overline{U}_{cl}$ which are presented at Figure 3.4. On the other hand, smaller differences to lesser extent on $\overline{u'v'}/\overline{U}_{cl}^2$

are presented at Figure 3.5. In view of the many possible explanations that may be offered for some of these disagreements between LDV and hot wire results, it is obvious that the most significant ones are: First, the LDV is a true one component device, whereas the hot wire is affected by all velocity components normal to the wire which limits its accuracy: especially in highly turbulent flows. The hot wire is also insensitive to velocity direction and becomes inaccurate at low velocities near the zero value. second, the seeding gradient problems associated with entrainment of unseeded ambient air affect LDV results as it will be explained later.

Generally speaking, it is obvious that both instruments predict the mean axial velocity. However, the measurements using both devices have the same trend and the same general features of the flowfield. The magnitude of the mean radial velocity using the LDV is higher. It is believed that this is because of seeding problems since only the air of the jet is seeded. The entrained air which is moving in the opposite radial direction is not seeded, and therefore its effect is not felt by the LDV. This could be the reason why the laser measurements are always higher.

In spite of the discrepancies of the radial velocity measurements, both instruments are probably satisfactory in view of the fact that the non-dimensional radial velocity is much smaller than the axial velocity and $\overline{V}/\overline{U}_o$ values does not exceed 4% in the far field or 7% in the near field. Again, these relatively high discrepancies in the radial velocity component when compared with axial velocity component could be because the LDV is entirely blind for the entrained fluid if it is not seeded

properly.

In the present investigation, it seems that velocity bias effects are not very important and the results do not change significantly, with or without correction. This is in agreement with what was reported earlier by Adams and Eaton [51] that several investigators have not found any bias effects in boundary layer type flows. In fact, they claimed that the uncorrected LDV is closer to the hot wire measurements than the corrected ones. The above argument is also supported by Buchhave [52] in a similar free jet study case. The implication of that is the magnitude of the LDV bias observed in their flow was not worse than the accuracy of the technique utilized in the same flow. Meyers and Wilkinson [53] have gone one step further by questioning the validity of using the velocity bias correction techniques. This is in contrast with Nejad and Davis [47] and also with Craig and Nejad [41] who confirmed the need for a correction even for flows with low turbulence levels.

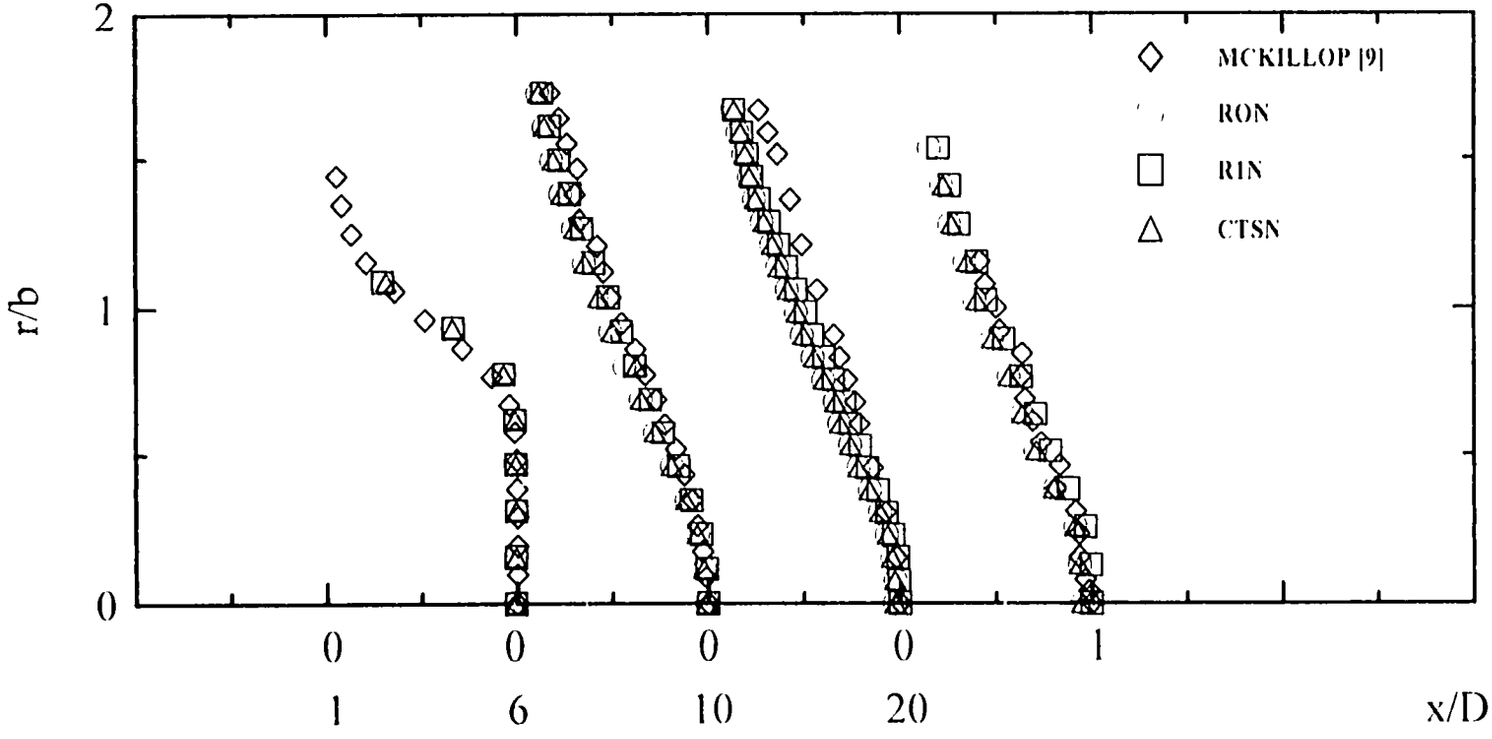

Figure 3.1: Comparision of axial mean velocity $\overline{U}_o/\overline{U}_{cl}$.

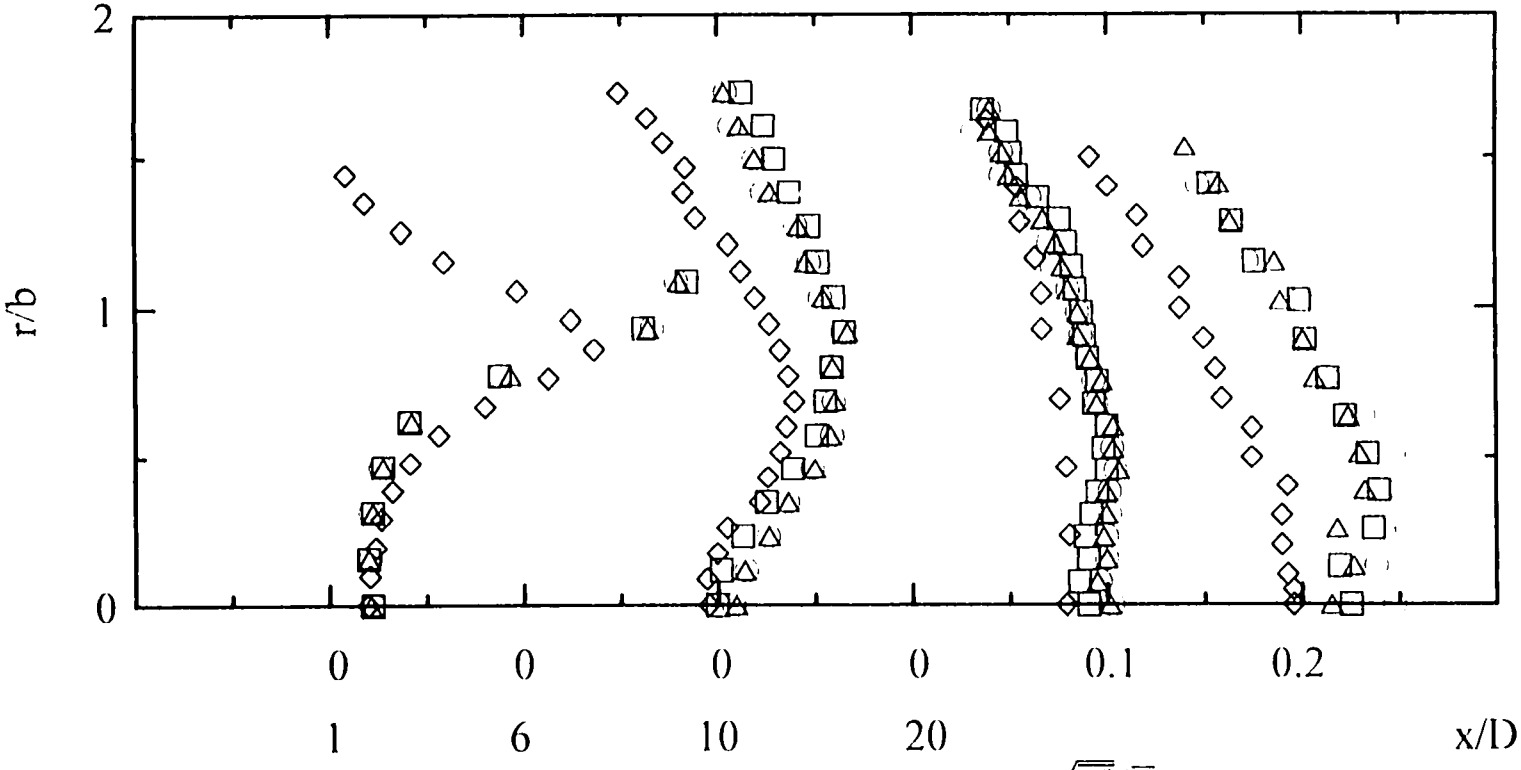

Figure 3.2: Comparision of turbulent axial velocity fluctuations $\sqrt{\overline{u'^2}}/\overline{U}_{cl}$; symbols are the same as in Figure 3.1.

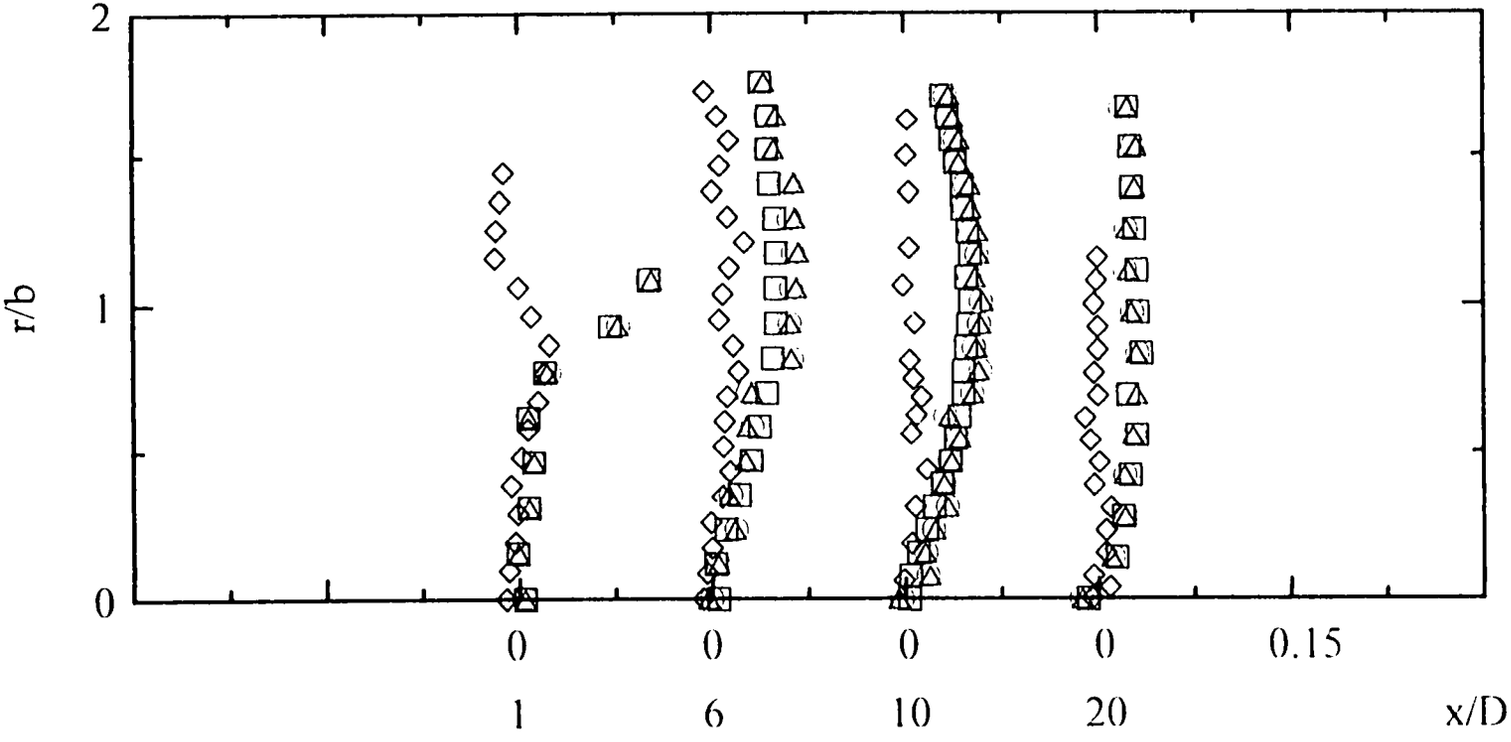

Figure 3.3: Comparision of radial mean velocity $\overline{V}_o/\overline{U}_d$; symbols are the same as in Figure 3.1.

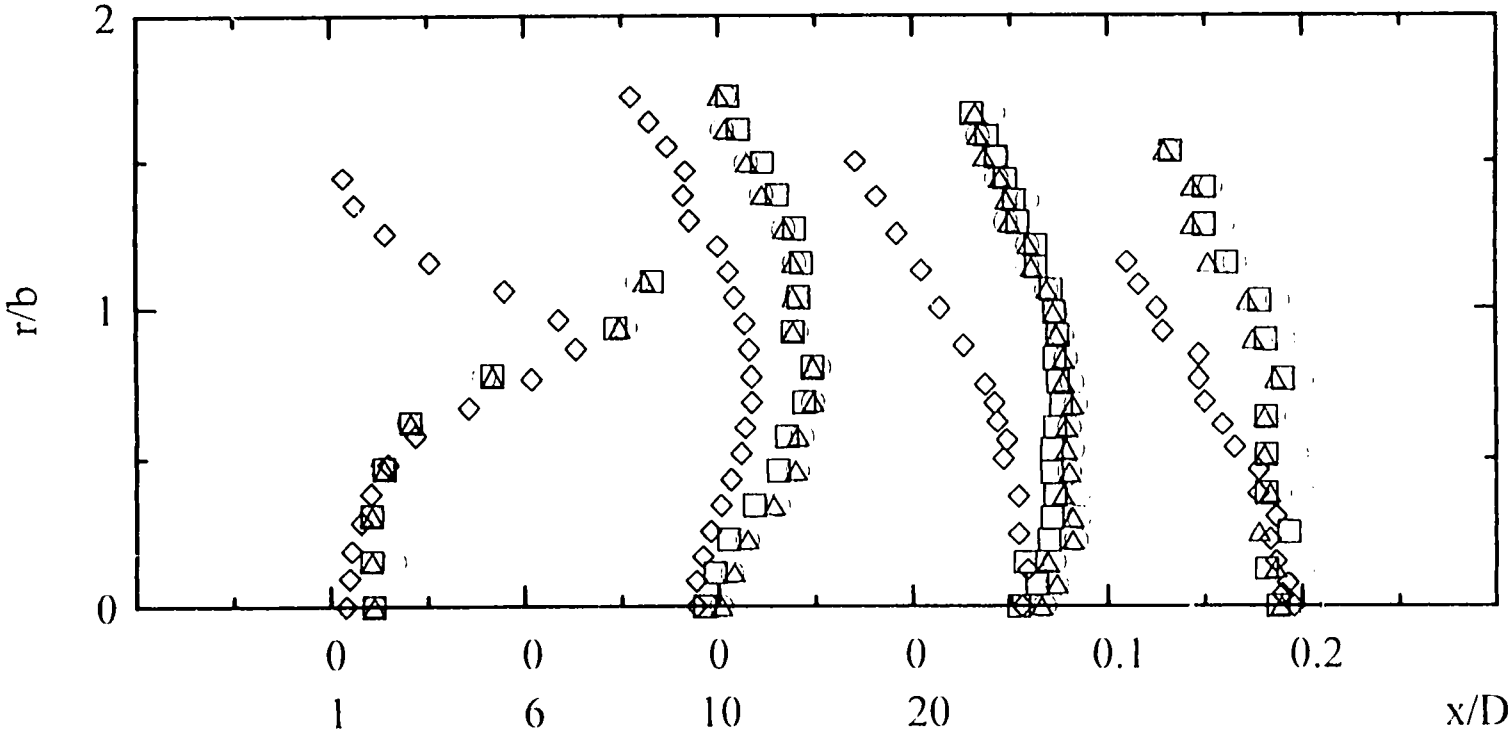

Figure 3.4: Comparision of turbulent radial velocity fluctuations $\sqrt{\overline{v'^2}}/\overline{U}_{cl}$; symbols are the same as in Figure 3.1.

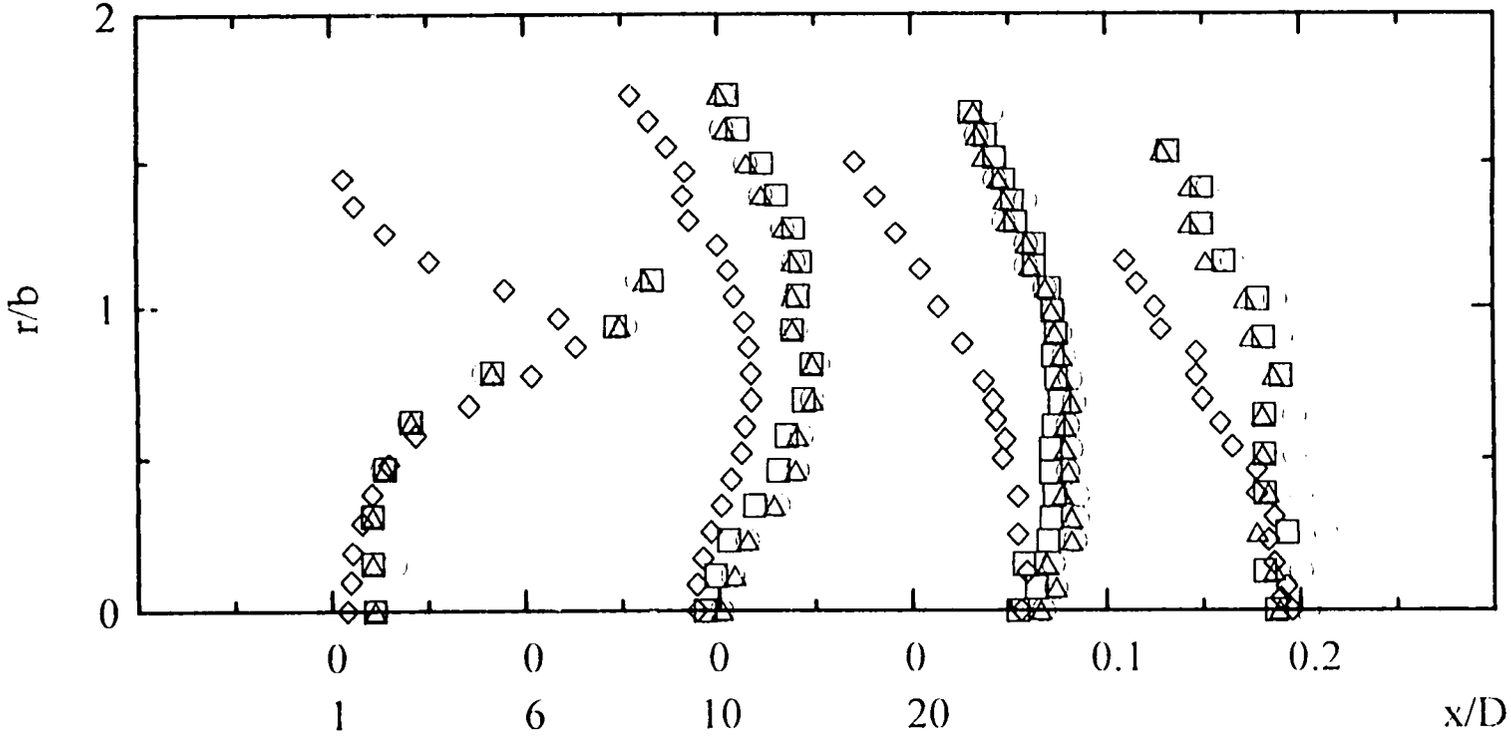

Figure 3.5: Comparision of turbulent shear stress $\overline{u'v'}/\overline{U}_d^2$; symbols are the same as in Figure 3.1.

Chapter 4

MEAN AND TURBULENT FLOW RESULTS

4.1 Centerline Results

For a self -preserving jet, the centerline velocity is given by George 1989 [54]:

$$\overline{U}_{cl} = BM_o^{\frac{1}{2}}/(x - x_o) \tag{4.1}$$

and,

$$\rho M_o = \frac{1}{4}\pi \overline{U}_o^2 D^2 \tag{4.2}$$

Where B is a constant and x_o represents a virtual origin. (note that both x_o and B values depend on the exit conditions). Also, ρM_o is the momentum flux, $\overline{U}_o$is the jet exit velocity and D is the jet exit diameter.

Substitute 4.2 in 4.1 and rearrange terms to get: where

$$\overline{U}_o/\overline{U}_{cl} = \frac{1}{B_u}[\frac{x}{D} - \frac{x_0}{D}] \tag{4.3}$$

where

$$B_u = \frac{1}{2}\pi^{\frac{1}{2}} B$$

The non dimensional centerline velocity $\overline{U}_o/\overline{U}_{cl}$is plotted as a function of axial location as shown in Figure 4.1. The jet exit velocity $\overline{U}_o$ and D jet diameter are used for normalizing the data. The above relation Equation 4.3 could be represented as a straight line on Figure 4.1. The greater the slope of this line indicates the higher the decay rate of the centerline velocity. The distance between the origin and the x-intercept of the straight line represents the virtual origin of the jet, x_o. The differences between the current data and others like Wyghanski & Fiedler [4] or Hussein [55] are the number of points used. For examples, the number of points which were taken by Wyghanski & Fiedler [4] and Hussein [55] covers 100 jet diameters, while current data covers 25 jet diameters . After curve fitting the current data, it was concluded that the present data's virtual origin is $x_o \approx 4D$ and the decay rate B $\approx$ 5.6. On the other hand Wyghanski & Fiedler's data [4] gave $x_o \approx 3D$ $B \approx 5.6$ or $B_u \approx 5.0$ while Hussein [52] data gave B $\approx$ 6.7 or $B_u \approx 5.9$: and $x_o \approx 2.7D$. The differences between the two cases where in the jet exit conditions.

Again, Figure 4.1 shows a typical centerline jet velocity characteristic which is

approximately constant for $x/D < 5$ (signifying the existence of a potential core) and followed by a region of rapid decay. The LDV velocity measurements are very close and the differences are probably within the experimental uncertainty of the device. It is obvious that the biased values are higher than the corrected values; especially, for $x/D > 14$. Figures 4.2 and 4.3 show the RMS turbulent velocity fluctuations as a function of axial distance measured from the exit of the jet. Evidence of increased mixing activities in the initial region of the jet can be observed from the behavior of both velocity components. As one moves farther downstream, the magnitude of turbulent velocity fluctuations increases gradually until it reaches to a constant value signifying the self-similar region value. The region of the greatest mean centerline velocity decay correspounds to higher velocity fluctuations which is an indication of maximum mixing activities at the end of the potential core and around the centerline region of the jet.

Where the peak values of $\sqrt{\overline{u'^2}}$ and $\sqrt{\overline{v'^2}}$ are compared, they were found to be approximately in the same axial location, but their magnitudes are different since $\sqrt{\overline{u'^2}}$ is slightly higher than $\sqrt{\overline{v'^2}}$ (*e.g*: $1.0 < \sqrt{\overline{u'^2}}/\sqrt{\overline{v'^2}} < 1.24$). This is an illustration of the near isotropy of the turbulence around the jet centerline. This Figure was not shown here for the sake of brevity

Generally speaking the comparisons between the three schemes for the centerline velocities shown in Figures 4.1 to 4.3, indicate little differences between the three methods.

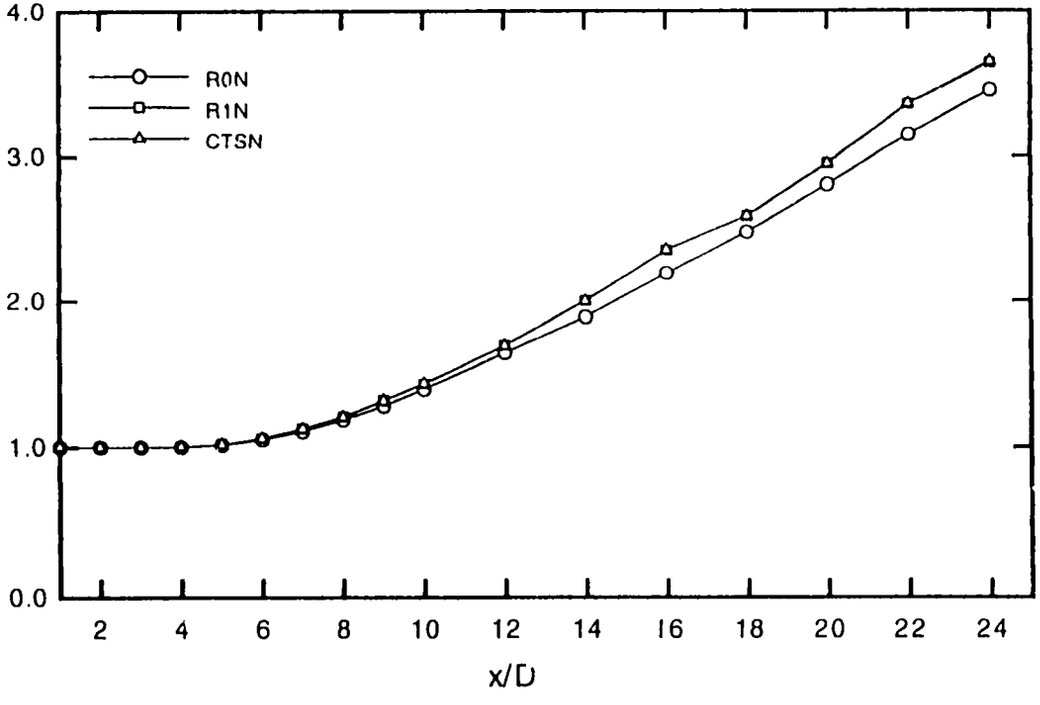

Figure 4.1: Variation of axial mean velocity $\overline{U}_o/\overline{U}_{oj}$ along the jet centerline.

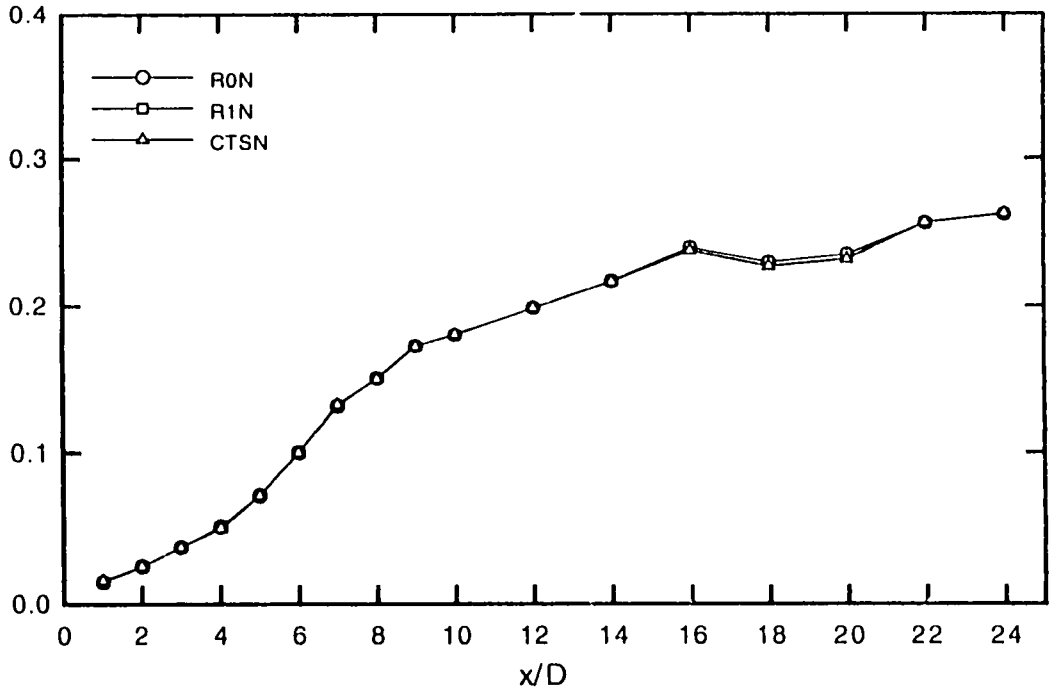

Figure 4.2: Variation of axial velocity fluctuations $\sqrt{\overline{u'^2}}/\overline{U}_{cl}$ along the jet centerline

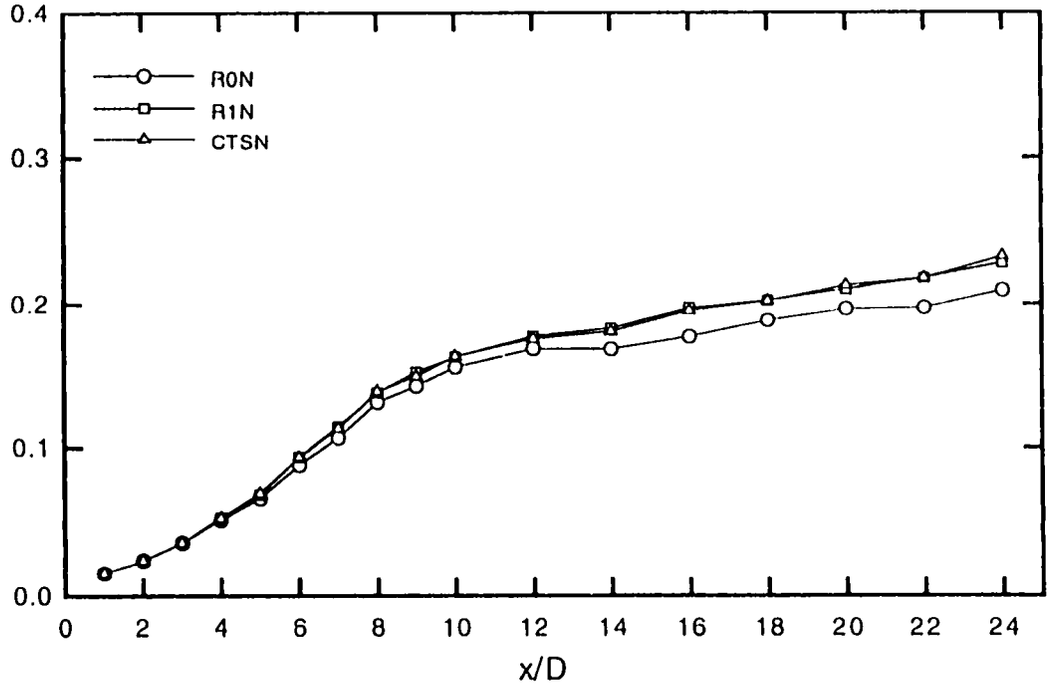

Figure 4.3: Variation of radial velocity fluctuations $\sqrt{\overline{v'^2}}/\overline{U}_{cl}$ along the jet centerline

4.2 Mean and Turbulent Flow Results.

Figures 4.4 to 4.8 show the radial distributions of the mean velocities, RMS turbulent fluctuations and shear stresses profiles at x/D = 1, 2, 4, 6, 8, 10, 12, 14, 16, 18, 20 and 22. For each of the above axial locations, three profiles are plotted. The previous techniques of LDV data processing are utilized to examine their agreement or differences, if any.

Figure 4.4 shows the evolution of the mean axial velocity profiles from x/D = 1 to x/D = 22. These results are typical of free jet data. The three schemes give approximately the same results. As expected, the biased data have slightly higher values.

Figure 4.5 shows the evolution of the axial RMS velocity fluctuations of the free jet. The off-center peaks are illustrated indicating the planes of maximum mixing. As expected, the biased data have slightly low values than their respective corrected ones. The differences between the corrected and the uncorrected data increase when the local turbulence increases. At the x/D = 2, 4 in Figures 4.5 and 4.7 the distribution of axial and radial turbulence intensities across the jet at the near field axial locations, the magnitude of the peak intensity and its radial location are in good agreement with the hot -wire results of Sami [8], who found peak intensities of $\sqrt{\overline{u'^2}}/\overline{U}_{cl} = 0.18$ and $\sqrt{\overline{v'^2}}/\overline{U}_{cl} = 0.15$ in a similar investigation.

Figure 4.7 represents the RMS of the radial velocity fluctuations which behaves

in a similar way to the RMS of the axial velocity fluctuations; however, their values are always slightly smaller except at the potential core of the jet (they have the same values).

Figure 4.8 shows the evolution of the turbulent shear stress variation $\overline{u'v'}/\overline{U}_o^2$ versus r/b. The results here show less scatter than Figures 4.5 and 4.7 .

The contours of axial velocity is shown in Figure 4.9. The axial is normalized by the jet exit velocity and the same thing for the other figures.

The contour lines of the velocity components and turbulence intensities are plotted in Figures 4.10 and 4.11. Here, contour lines show more details about the flowfield and give a visual impression of the flow, and therefore, were plotted to help in the interpretation of the data. Figure 4.9 show contour lines of axial velocities which are typical of free jet flows (see Chen et al.[56]). The spread of the jet and the increase of its size is clear in all Figures 4.9 to 4.12. Figure 4.10 shows the contours of axial turbulence intensity $\sqrt{\overline{u'^2}}/\overline{U}_o$. Agian, the potential core with minimum disturbances is well defined (0.04 turbulence intesity level). Some of the contoure (0.16 value) form island shape contours which are charactristics of free jet flow (see Chen et al [56].). Some others, the islands are not complete (0.12 value) because half of the jet flow is only plotted. Most of there contours merge around the jet exit r/D = 0.5 where most of the changes originate at that plane. Figure 4.12 shows the contours of radial turbulence intensity $\sqrt{\overline{v'^2}}/\overline{U}_o$ contours looks very similar to that of $\sqrt{\overline{u'^2}}/\overline{U}_o$ contours but contour lines of the same value are relatively shorter. The

locus of the maximum appears to be near identical to the locus of $\sqrt{v'^2}/\overline{U}_o$. The contours of $\overline{u'v'}/\overline{U}_0^2$ are shown in Figure 4.12. Agian, The locus of maxima seem to follow those of $\overline{u'v'}/\overline{U}_0^2$ or $\sqrt{u'^2}/\overline{U}_o$ confirming that most of the radial changes happen at the same planes of high velocity gradients.

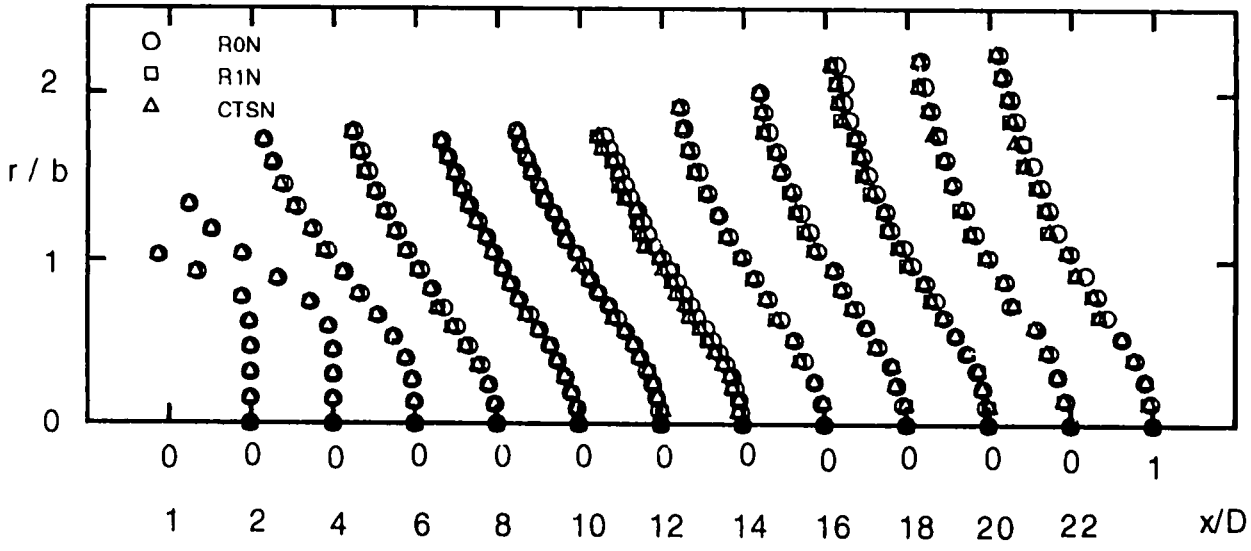

Figure 4.4: Evolution of axial velocity; $\overline{U}/\overline{U}_{cl}$.

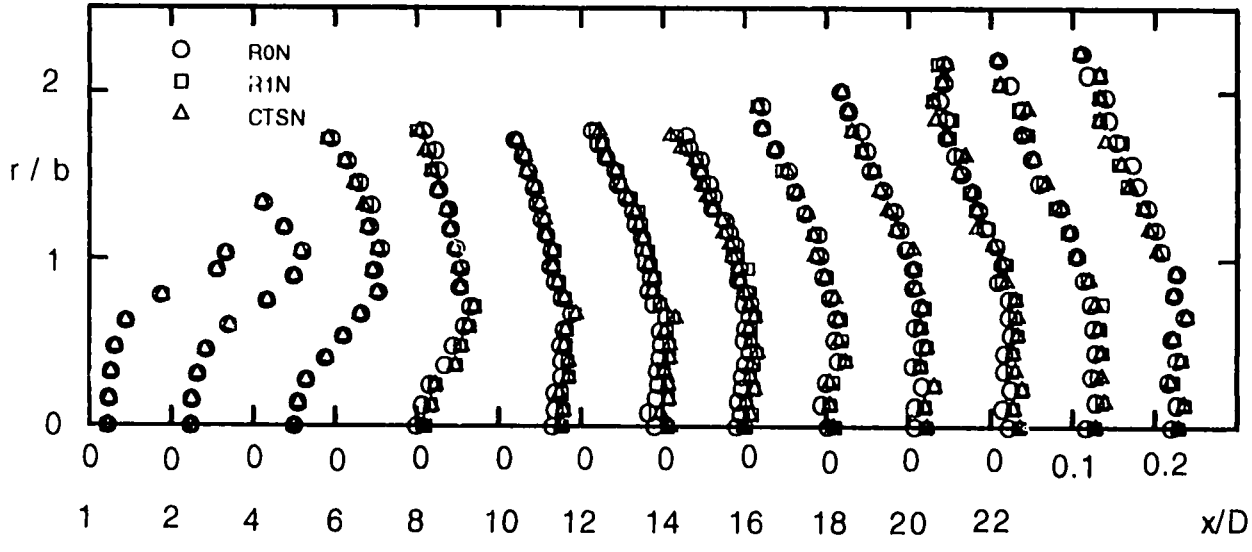

Figure 4.5: Evolution of axial velocity fluctuations; $\sqrt{\overline{u'^2}}/\overline{U}_{el}$

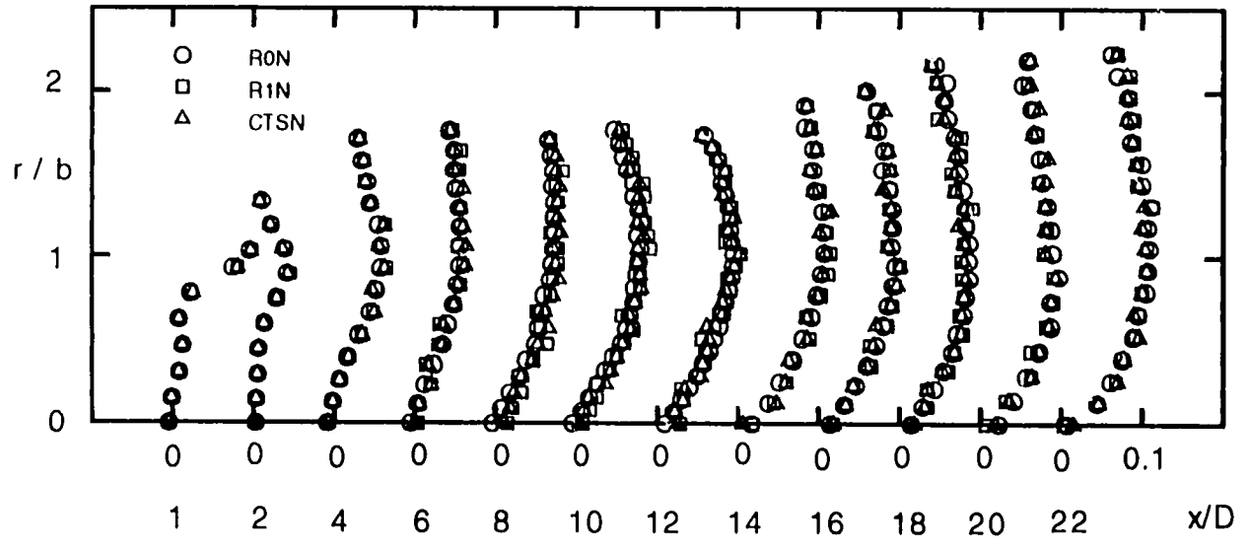

Figure 4.6: Evolution of radial velocity, $\overline{V}/\overline{U}_a$

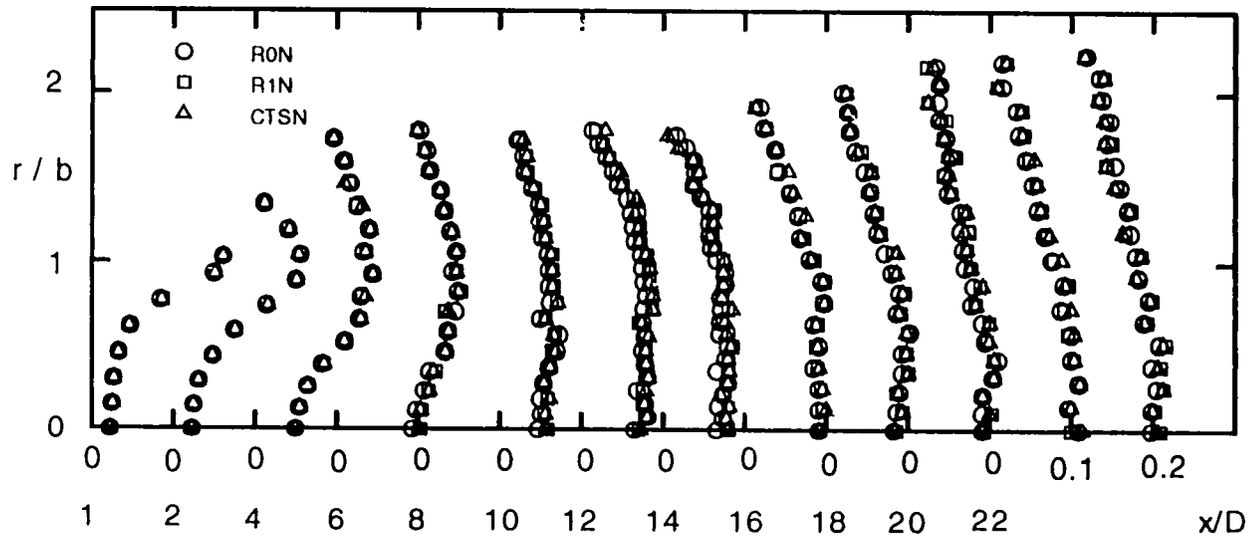

Figure 4.7: Evolution of radial velocity fluctuations; $\sqrt{\overline{v'^2}}/\overline{U}_{cl}$.

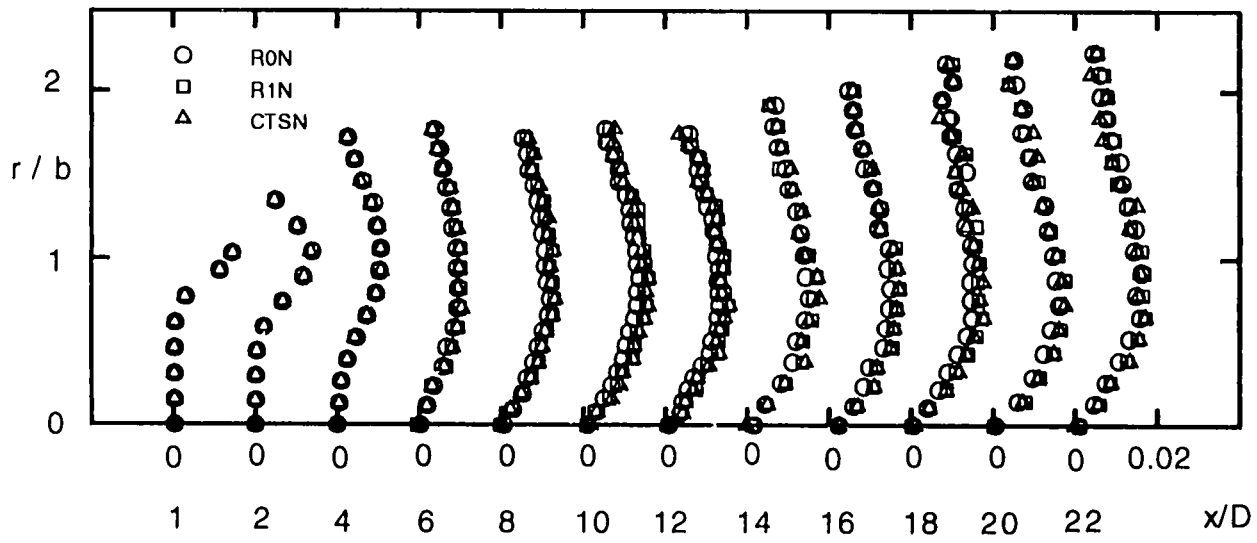

Figure 4.8: Evolution of shear stresses; $\sqrt{\overline{u'v'}}/\overline{U}_{cl}^2$.

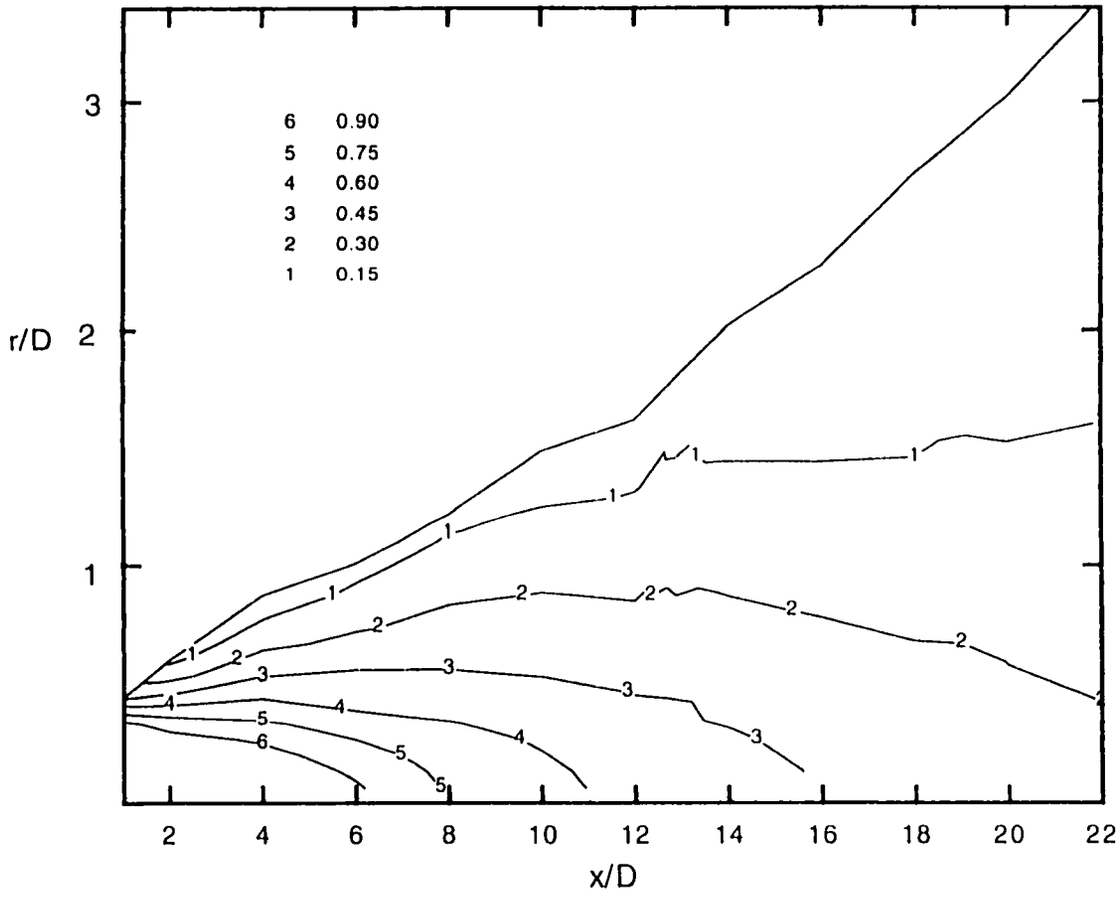

Figure 4.9: Contours of axial mean velocity $\overline{U}/\overline{U}_o$

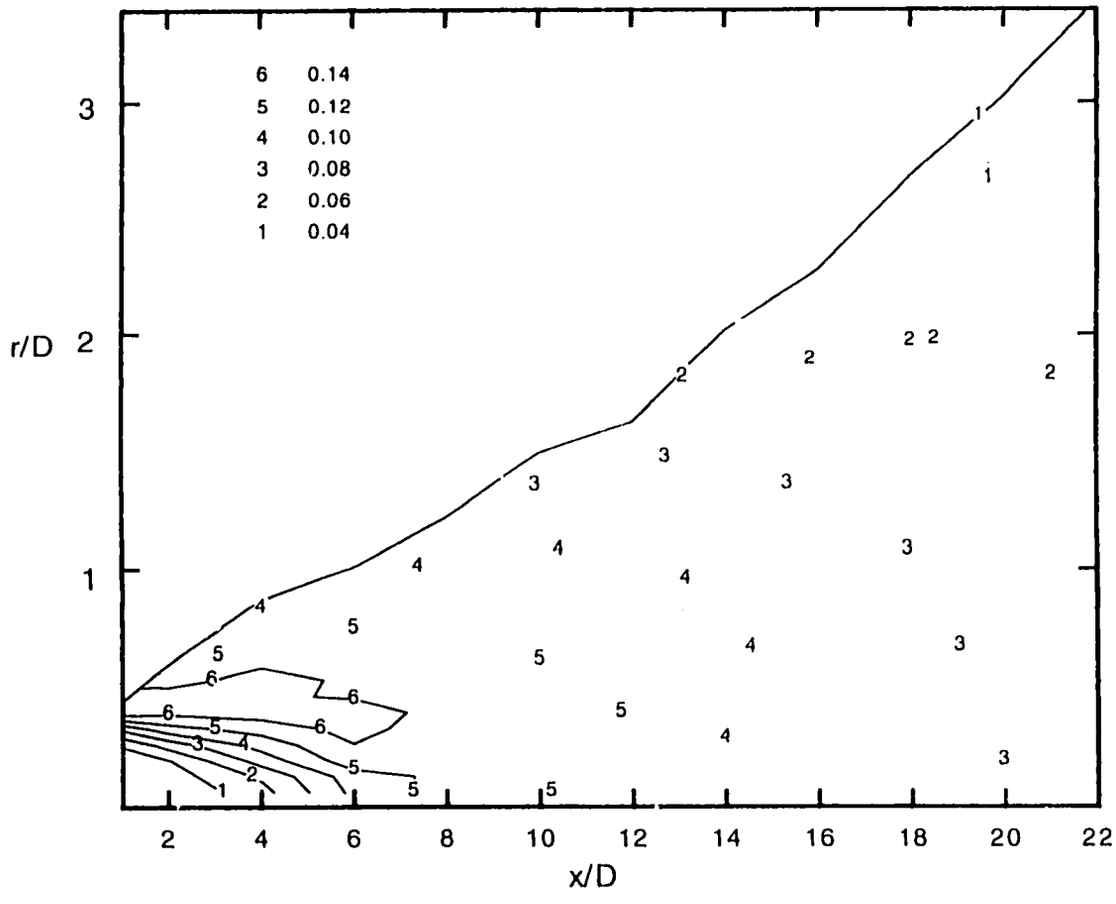

Figure 4.10: Contours of axial velocity fluctuations $\sqrt{\overline{u'^2}}/\overline{U}_o$

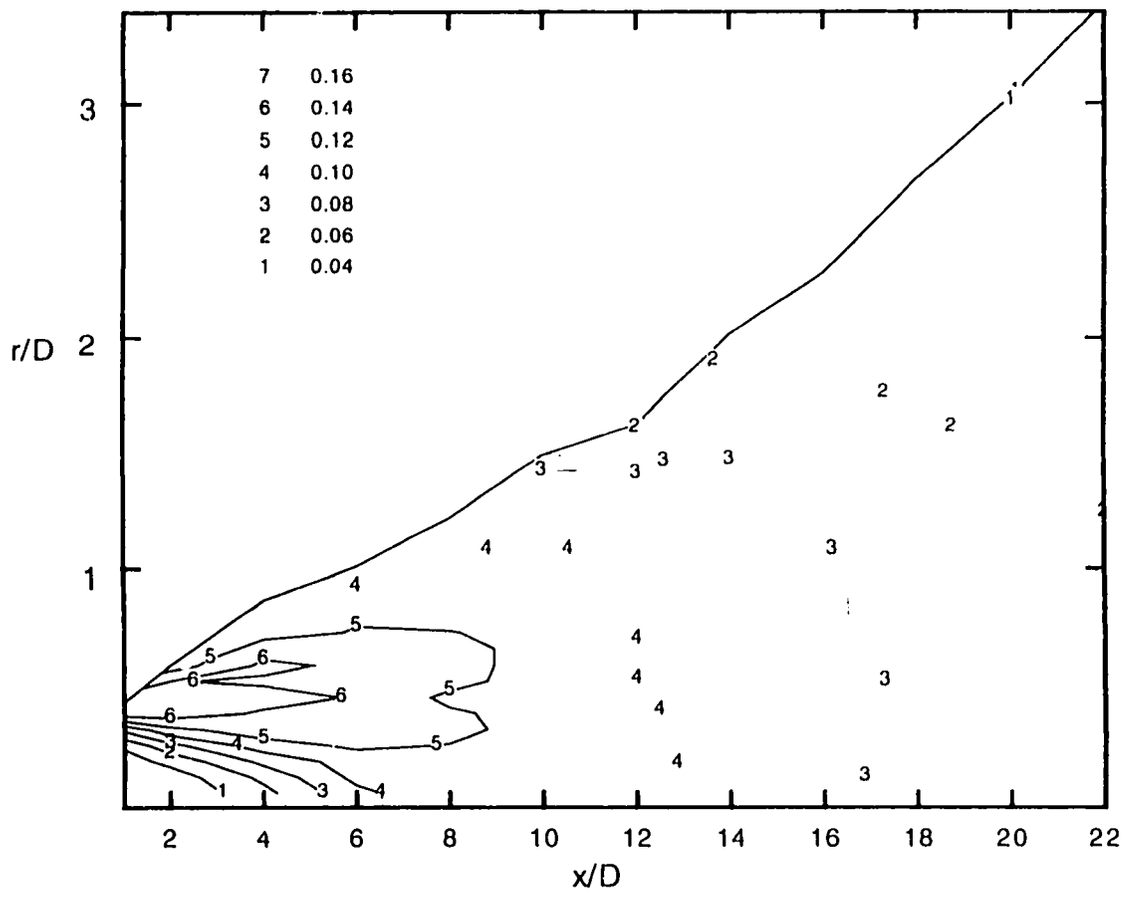

Figure 4.11: Contours of radial velocity fluctuations $\sqrt{\overline{v'^2}}/\overline{U}_o$

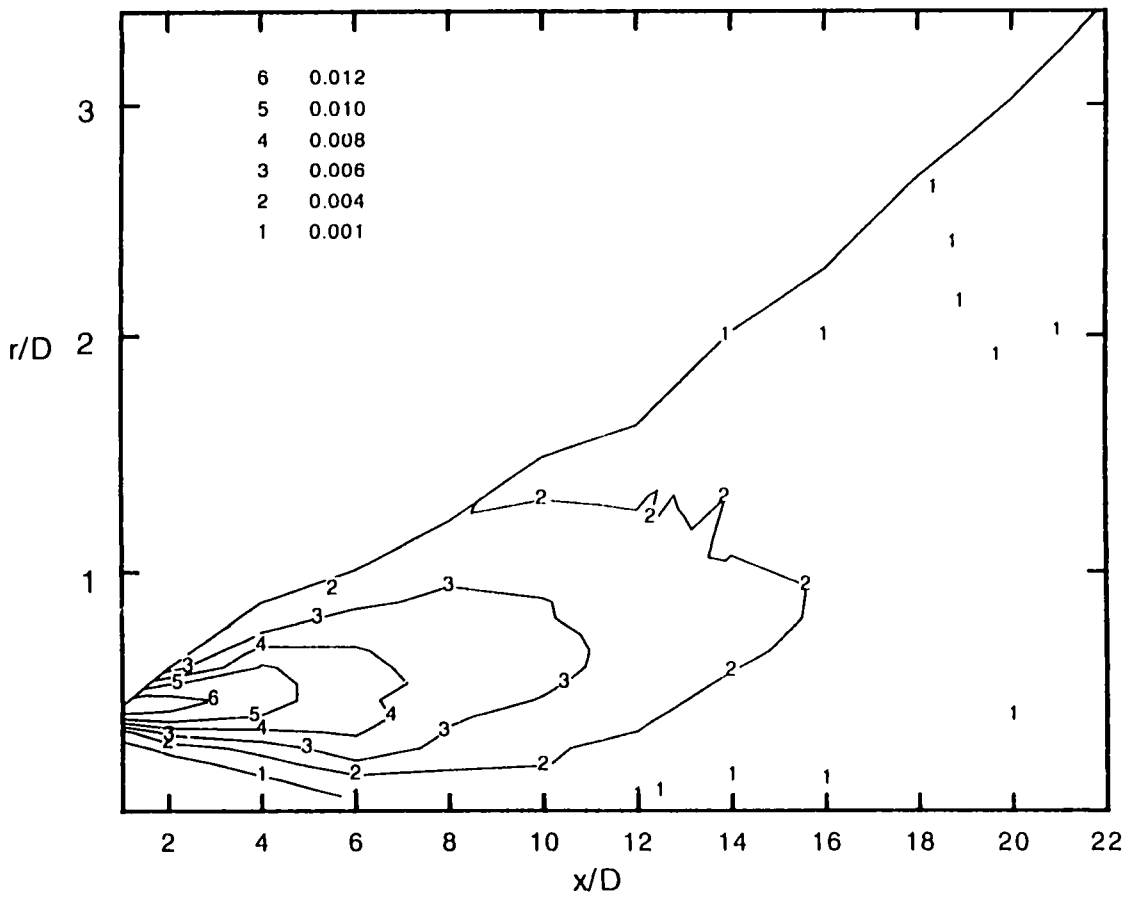

Figure 4.12: Contours of shear stresses $\overline{u'v'}/U_o^2$

4.3 Triple Product Results.

The turbulent triple products that were measured in this study are $\overline{u'^3}$,$\overline{u'^2v'}$, $\overline{u'v'^2}$ and $\overline{v'^3}$. and others were not measured because the LDV system was not a 3-D system. The normalized values are shown in Figures 4.13 to 4.16.

If correlation for $\overline{u'v'^2}$ is considered to be the radial transport of the shear stress $\overline{u'v'}$. then the measured behavior implies essentially gradient flux of $\overline{u'v'}$. This gradient transport would require negative values of $\overline{u'v'^2}$ inside the location of maximum shear and positive values outside as reported by (Amano et al. [57]). In other words, a sign change takes place approximately where the second-order quantities (i.e.. normal or shear stress) have their maxima. Similar arguments are true for the rest of the triple products.

The triple products have certain common characteristics. For example, they peak at shear layer and their values diminishes at the edges of the shear layer. These peaks are more prominent and sharp in the near field while they decrease in value and increase in size downstream. A similar behavior of the triple velocity product terms was observed by Gould et al. [58] for a confined jet.

The most noticeable feature of the experimental observations reported by Chandrsuda and Bradshaw [60] and later by Driver and Seegmiller [61] is that the shapes of the third-order moments of turbulence fluctuating velocity change rapidly along the separated shear layer due to distortion of the large eddies by effectively irrota-

tional mechanisms.

Figure 4.13 to 4.16 show peaks at the shear layer and approaching zero at the edges of the shear layer. This behavior is characteristic of free shear layers in early stages of separation.

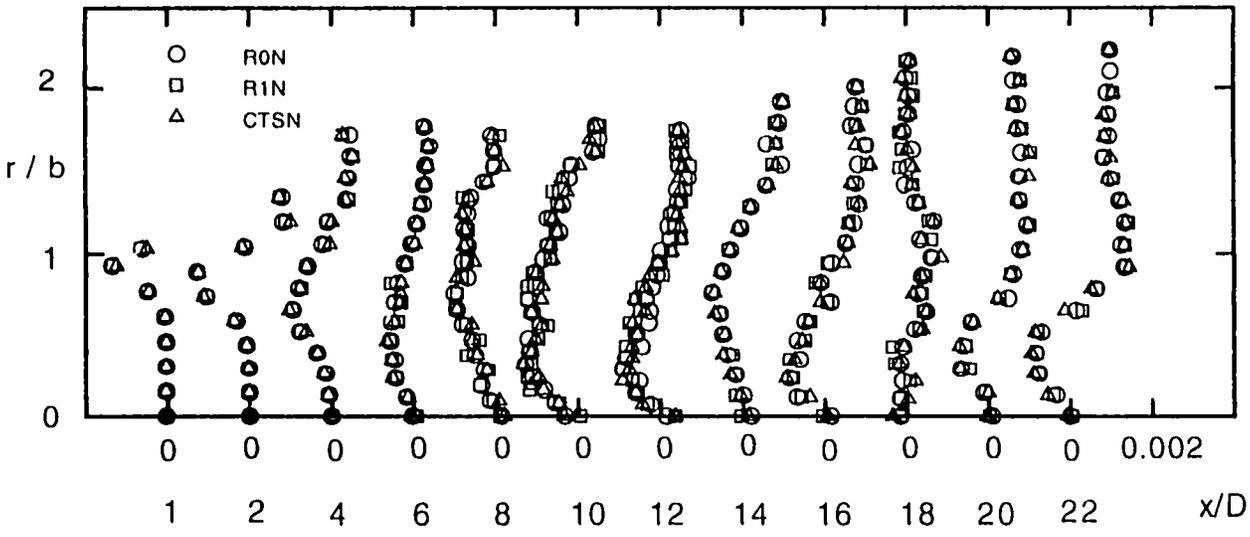

Figure 4.13: Evolution of non-dimensional triple velocity correlations, $\overline{u^3}/\overline{U}_d^3$.

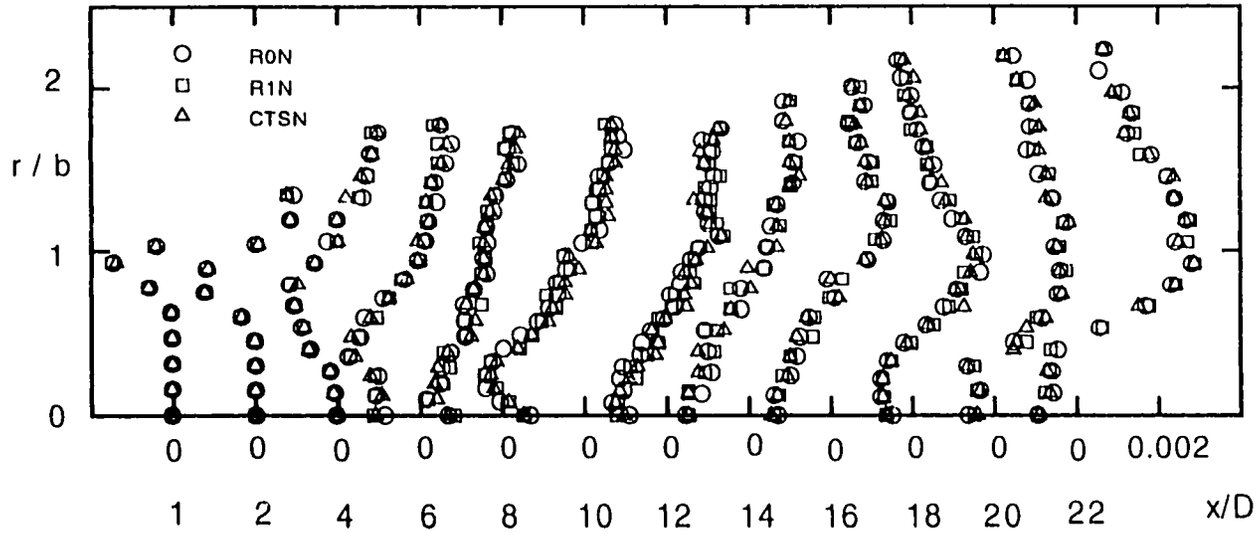

Figure 4.14: Evolution of non-dimensional triple velocity correlations, $\overline{v^3}/\overline{U}_{cl}^3$.

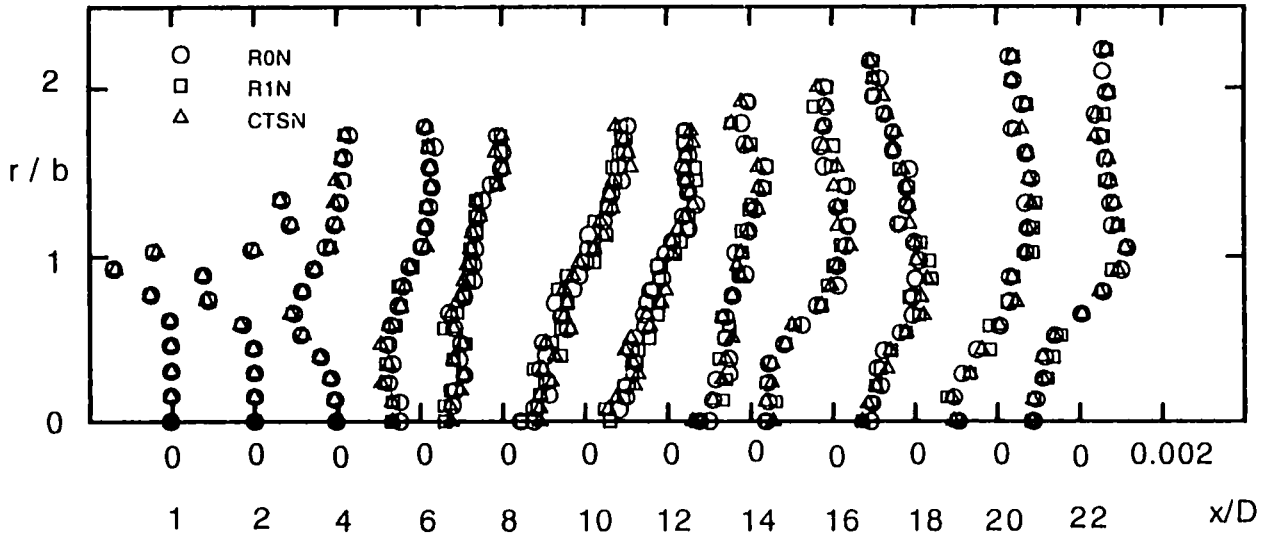

Figure 4.15: Evolution of non-dimensional triple velocity correlations, $\overline{u'^2v'}/\overline{U}_d^3$.

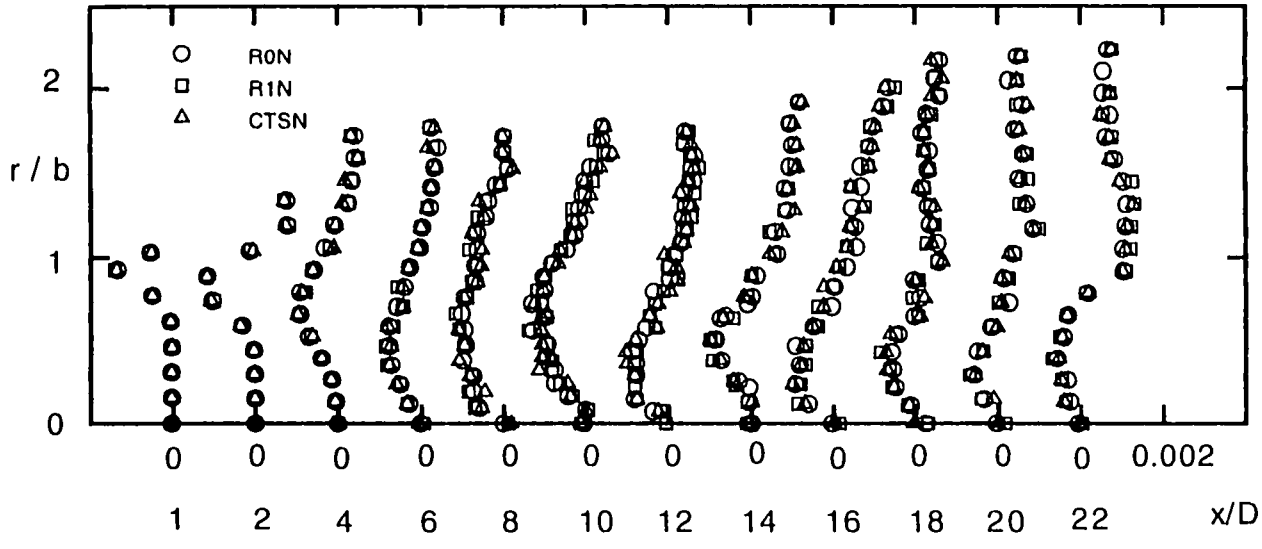

Figure 4.16: Evolution of non-dimensional triple velocity correlations, $\overline{u'v'^2}/\overline{U}_{cl}^3$.

Chapter 5

TURBULENT KINETIC ENERGY RESULTS

5.1 Turbulent Kinetic Energy (TKE) Equation

The experimental data were analyzed for the turbulent kinetic energy terms: production, diffusion, convection, and viscous dissipation. Since axisymmetry was assumed for the flow (this was seen as a valid assumption from the experimental results), a two dimensional cylindrical coordinate system was used. The modeled domain was from the inlet of the jet to the last measurement plane, that is, $x/D = 1$ *to* 22. The turbulence energy equation in cylindrical coordinates (for steady, axisymmetric, and constant density flow), employed in the determination of the turbulent kinetic energy terms in this analysis, could be written as (see Appendix A and B for the

derivation of this equation)

$$\overline{U}\frac{\partial k}{\partial x}+\overline{V}\frac{\partial k}{\partial r} = \frac{1}{\overline{\rho}}\frac{\partial}{\partial x}\left[\mu\frac{\partial k}{\partial r}-\overline{\rho}\frac{\overline{u'v'^2}}{2}-\overline{\rho}\frac{\overline{u'u'^2}}{2}-\overline{\rho}\frac{\overline{u'^3}}{2}-\overline{u'p'}\right]+ \frac{1}{\overline{\rho}r}\frac{\partial}{\partial r}\left[\mu r\frac{\partial k}{\partial r}-\overline{\rho}r\frac{\overline{v'^3}}{2}-\overline{\rho}r\frac{\overline{v'u'^2}}{2}-\overline{\rho}r\frac{\overline{u'^2v'}}{2}-r\overline{v'p'}\right]-\left[\frac{\mu\overline{v'^2}}{\overline{\rho}r^2}+\frac{\mu\overline{u'^2}}{\overline{\rho}r^2}\right]- \left[\overline{v'^2}\frac{\partial\overline{V}}{\partial r}+\overline{u'v'}\frac{\partial\overline{U}}{\partial r}+\overline{u'v'}\frac{\partial\overline{V}}{\partial x}+\overline{u'^2}\frac{\partial\overline{U}}{\partial x}+\overline{u'^2}\frac{\overline{V}}{r}-\overline{u'w'}\frac{\partial\overline{W}}{\partial x}+\overline{v'w'}\frac{\partial\overline{W}}{\partial r}+\overline{v'w'}\frac{\overline{W}}{r}\right]- \frac{\mu}{\overline{\rho}}\left[\overline{\left(\frac{\partial v'}{\partial r}\right)^2}+\overline{\left(\frac{\partial u'}{\partial r}\right)^2}+\overline{\left(\frac{\partial u'}{\partial r}\right)^2}+\overline{\left(\frac{\partial v'}{\partial x}\right)^2}+\overline{\left(\frac{\partial u'}{\partial x}\right)^2}-\overline{\left(\frac{\partial u'}{\partial x}\right)^2}\right]$$

The first line of the equation represents "CT", the second and third lines of the equation represent "DT" while the fourth line represent "PT" and the fifth line represent "VDT".

The equation is composed of the following terms:

1. axial and radial convection of turbulent kinetic energy

$$\overline{U}\frac{\partial k}{\partial x}+\overline{V}\frac{\partial k}{\partial r}$$

2. axial diffusion of turbulent kinetic energy

$$\frac{1}{\overline{\rho}}\frac{\partial}{\partial x}\left[\mu\frac{\partial k}{\partial x}-\overline{\rho}\frac{\overline{u'v'^2}}{2}-\overline{\rho}\frac{\overline{u'u'^2}}{2}-\overline{\rho}\frac{\overline{u'^3}}{2}-\overline{u'p'}\right]$$

3. radial diffusion of turbulent kinetic energy

$$\frac{1}{\overline{\rho}r}\frac{\partial}{\partial r}\left[\mu r\frac{\partial k}{\partial r}-\overline{\rho}r\frac{\overline{v'^3}}{2}-\overline{\rho}r\frac{\overline{v'u'^2}}{2}-\overline{\rho}\frac{\overline{u'^2v'}}{2}-r\overline{v'p'}\right]$$

4. additional terms which are usually very small relative to other terms

$$\frac{\mu\overline{v'^2}}{\overline{\rho}r^2} + \frac{\mu\overline{u'^2}}{\overline{\rho}r^2}$$

5. production of turbulent kinetic energy

$$\overline{v'^2}\frac{\partial\overline{V}}{\partial r} + \overline{u'v'}\frac{\partial\overline{U}}{\partial r} + \overline{u'v'}\frac{\partial\overline{V}}{\partial x} + \overline{u'^2}\frac{\partial\overline{U}}{\partial x} + \overline{w'^2}\frac{\overline{V}}{r} + \overline{u'w'}\frac{\partial\overline{W}}{\partial x} + \overline{v'w'}\frac{\partial\overline{W}}{\partial r} + \overline{v'w'}\frac{\overline{W}}{r}$$

6. viscous dissipation of turbulent kinetic energy

$$\frac{\mu}{\overline{\rho}}\left[\overline{\left(\frac{\partial v'}{\partial r}\right)^2} + \overline{\left(\frac{\partial w'}{\partial r}\right)^2} + \overline{\left(\frac{\partial u'}{\partial r}\right)^2} + \overline{\left(\frac{\partial v'}{\partial x}\right)^2} + \overline{\left(\frac{\partial w'}{\partial x}\right)^2} + \overline{\left(\frac{\partial u'}{\partial x}\right)^2}\right]$$

5.2 Calculation Procedure

All the terms of the turbulent kinetic energy are calculated from the experimental data except the viscous dissipation terms, which were obtained by algebraic energy balance of the turbulent kinetic energy equation.

To calculate each term in the turbulence energy equation using experimental data, first and second derivatives have to be evaluated. For example, central differences were used to calculate the first derivatives while the second derivatives were estimated using the method of undetermined coefficients as reported by Lapidus and Pinder [62]. This method takes care of the non-uniformity in spacing along the x and r axes. The method is also valid for uniform grid (e.g., when the method of undetermined coefficients is used for equal spacing of points, its result is the same

as the conventional method. The descretized expression for the second derivatives of k with respect to a coordinate axis x at a location (i, j), using the method of undetermined coefficient, is as follows:

$$\frac{\partial^2 k_{i,j}}{\partial x^2} = a_{i-1,j}\, k_{i+1,j} + a_{i,j}\, k_{i,j} + a_{i-1,j}\, k_{i-1,j}$$

where

$$a_{i,j} = \left(\frac{\Delta x_1^2}{2} + \frac{\Delta x_2 \Delta x_1}{2} \right)^{-1},$$

$$a_{i-1,j} = \left(\frac{\Delta x_2^2}{2} + \frac{\Delta x_2 \Delta x_1}{2} \right)^{-1}, \text{and}$$

$$a_{i-1,j} = -1.0 * (a_{i,j} + a_{i-1,j})$$

while,

$$\Delta x_1 = x_i - x_{i-1},$$

and

$$\Delta x_2 = x_{i+1} - x_i$$

A computer program, written in fortran language, was developed to calculate the required TKE terms.

5.3 Turbulent Kinetic Energy Results

Figures 5.1 to 5.6 show the profiles of the TKE terms of the jet. Figure 5.1 shows profiles of the total non-dimentional production term "PT" (normalized by $\overline{U}_0^3$).

The plots show that the profiles have peaks around the shear layers. Generally, the values of the peak decay downstream of the jet, dying out completely downstream of x = 8D. The production term make positive contributions to the TKE and its peak (i.e. maximum production rate) decreases with increasing stream wise distance.

The production term $-\overline{u'v'}\frac{\partial U}{\partial r}$ was found to dominate the total production term(see Figure C.4). On the other hand,- $\overline{v'^2}\frac{\partial V}{\partial r}$ and $-\overline{u'^2}\frac{\partial U}{\partial x}$, terms made opposite contribution to the production.

The total non-dimensional convection term "CT" profiles are shown in Figure 5.2. The plots of "CT" profiles are characterized with a sine wave distribution observed around the center of the shear layer. These peaks diminish downstream of the jet exit at approximately $x/D > 10$. Hence, energy is convected, and as such carried, from around the center of the shear layer toward the shear layer edges.

The turbulent total non-dimensional diffusion term "DT" , whose profiles are shown in Figure 5.3, redistributes the energy in the vicinity of the shear layer from the centers to the outer parts of the shear layer. The dominant part of the total diffusion are $\frac{1}{\rho}\frac{\partial}{\partial x}\left(-\rho\frac{\overline{u'^3}}{2}\right)$ and $\frac{1}{\rho}\frac{\partial}{\partial x}\left(-\rho\frac{\overline{u'v'^2}}{2}\right)$ as appears in Figures C.11 and C.12.

Figure 5.4 shows the total non-diminensional viscous dissipation term "VDT", obtained from the balance of the TKE transport equation, is seen to make a negative contribution to TKE (i.e. loss) and portrays a similar but opposite profile style as the production term .

Figure 5.5 shows the non-isotropic factor which defined as "NIF". Figure 5.6

shows the turbulent kientic energy distribution through the entire flow field.

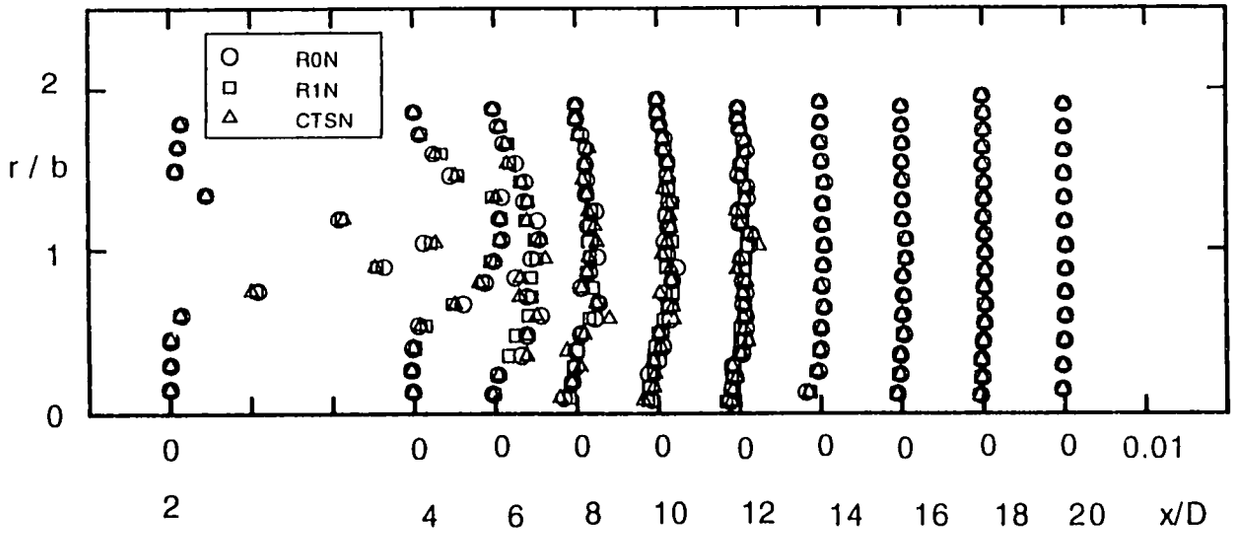

Figure 5.1: Evolution of total turbulance production "PT".

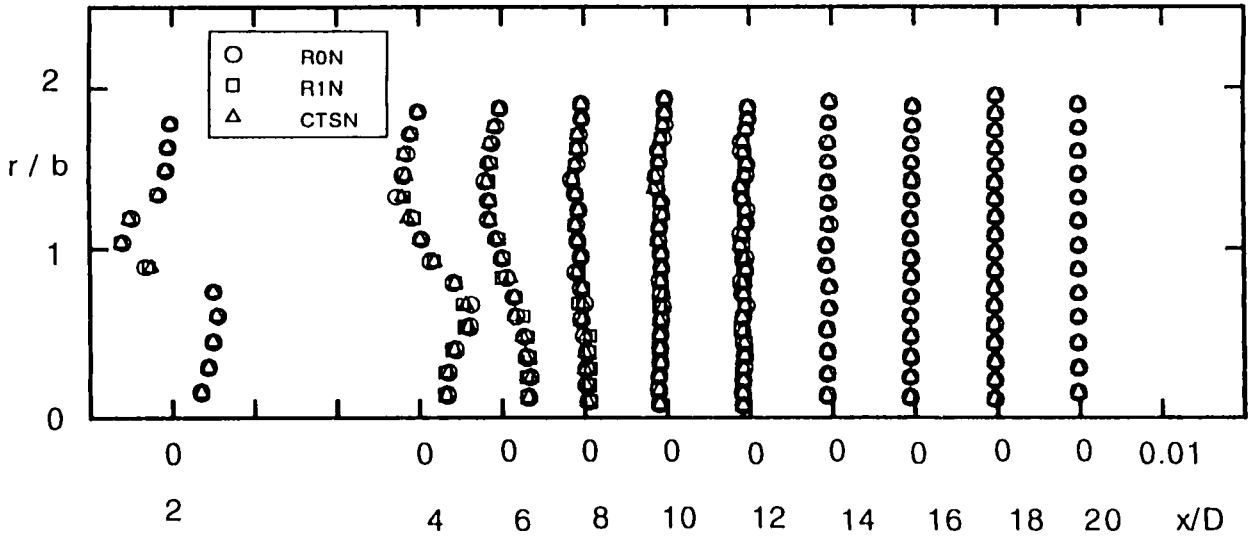

Figure 5.2: Evolution of total turbulance convection "CT".

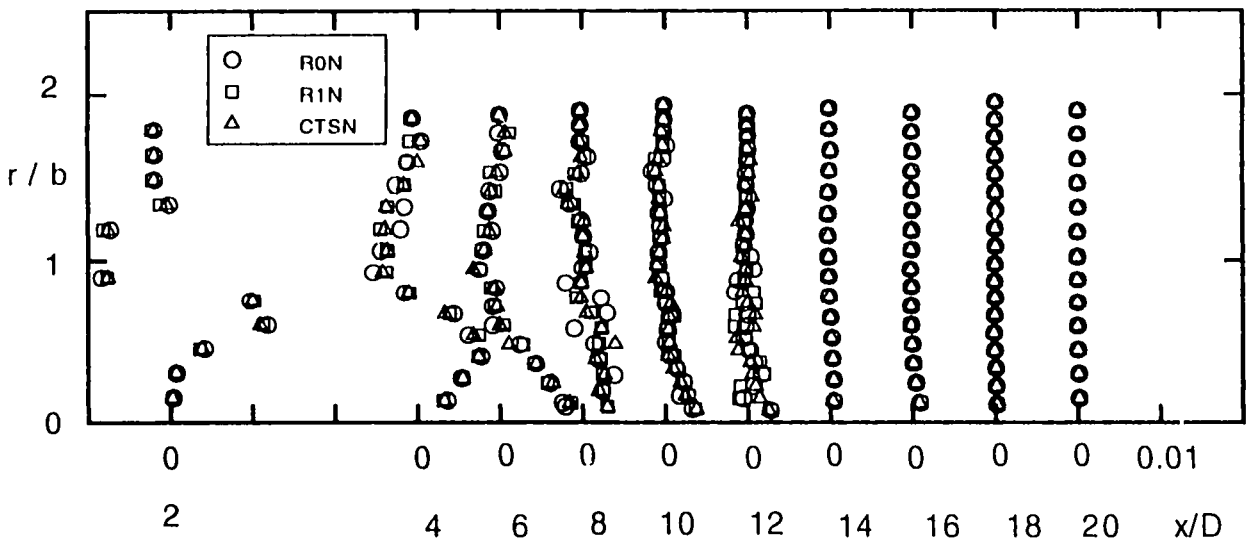

Figure 5.3: Evolution of total turbulance diffusion "DT".

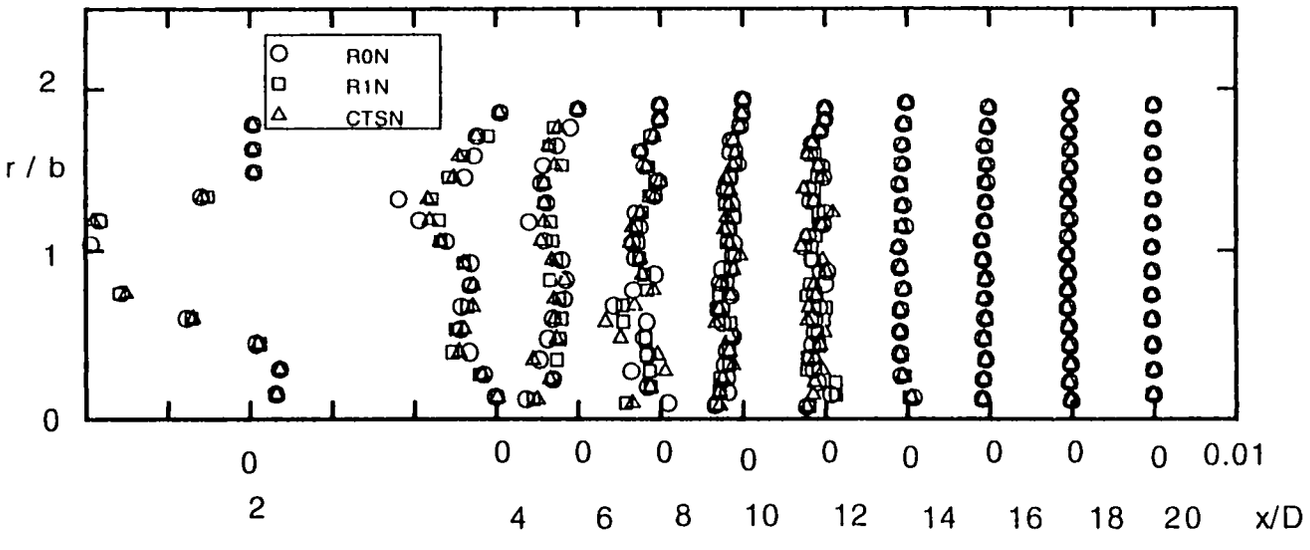

Figure 5.4: Evolution of total turbulance viscous dissipation "VDT".

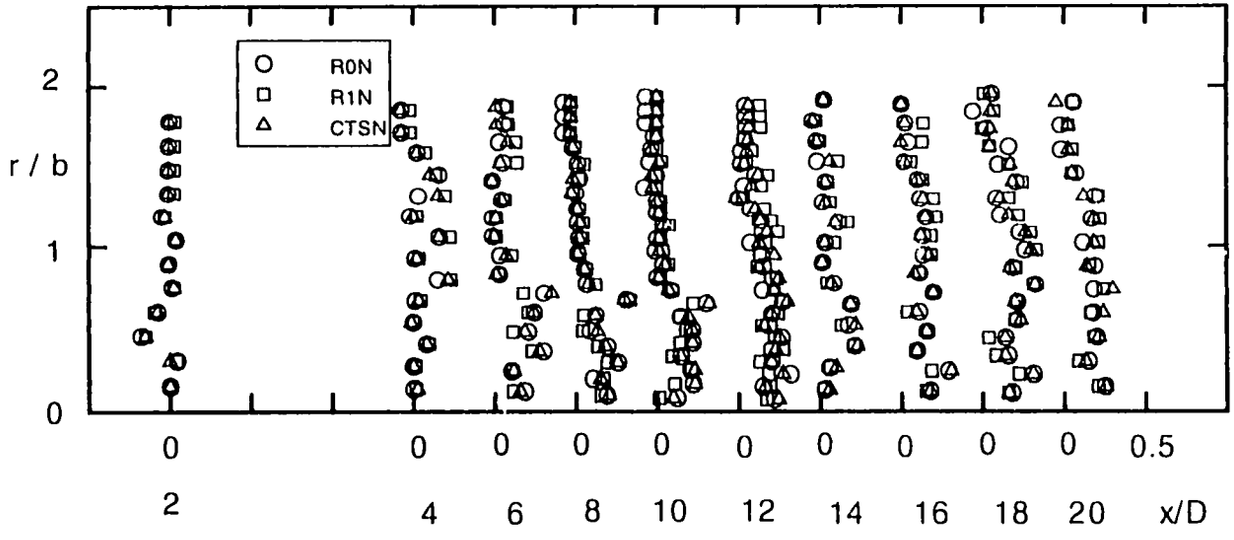

Figure 5.5: Evolution of total turbulance non-isotropic factor "NIF".

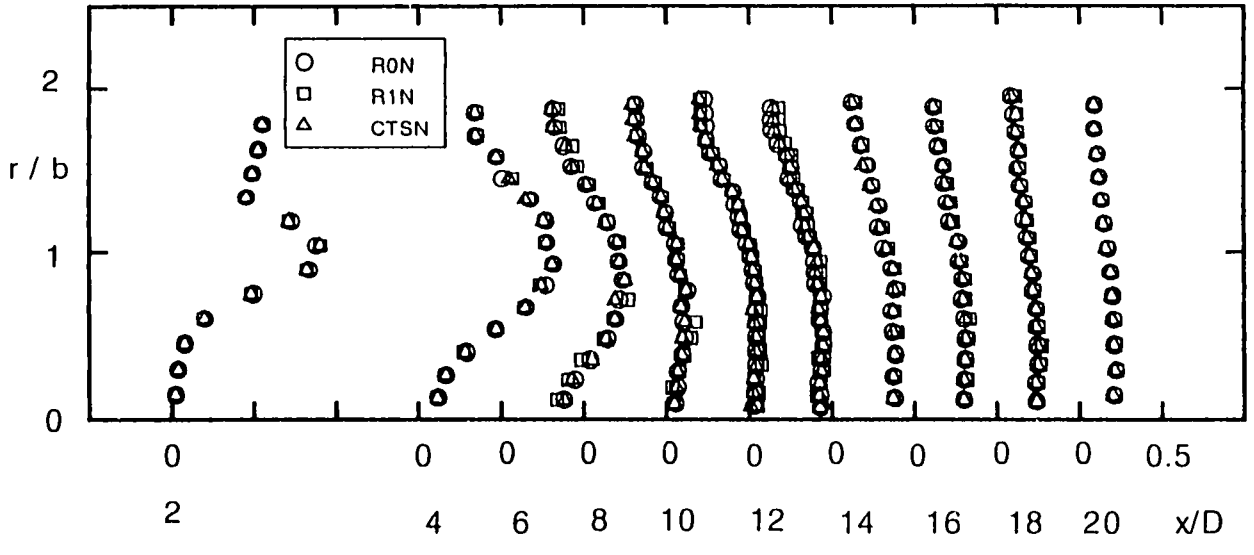

Figure 5.6: Evolution of total turbulance kienetic energy "K".

Chapter 6

CONCLUSIONS

A two component LDV in the coincidence mode was utilized in a novel experimental arrangement to obtain and document detailed experimental data in the near, intermediate and far field of a free jet. Three different methods to analyze the data were used: namely, the arithmetic average, the interarrival time weighting, and constant time sampling. Comparisons between these different methods indicate that bias effects are insignificant for the present experimental data. The results indicate the significant effects of the turbulent shear layer and its responsibilites in turbulence production and enhancing mixing. As a result, energy was distributed in a very short distance. Finally, these detailed information in the nearfield of a free jet should be of value for further development of second order closure models.

APPENDIX

Table .1: Abbreviations used for component parts of the TKE terms

TKE Terms	Abbreviations	Mathematical Expressions
Production	P1	$-\overline{v'^2}\frac{\partial \overline{V}}{\partial r}$
	P2	$-\overline{u'^2}\frac{\partial \overline{U}}{\partial x}$
	P3	$-\overline{u'v'}\frac{\partial \overline{V}}{\partial x}$
	P4	$-\overline{u'v'}\frac{\partial \overline{U}}{\partial r}$
Convection	C1	$\overline{U}\frac{\partial k}{\partial x}$
	C2	$\overline{V}\frac{\partial k}{\partial r}$
Diffusion	D1	$\frac{1}{\rho r}\frac{\partial}{\partial r}\left(\mu r\frac{\partial k}{\partial r}\right)$
	D2	$\frac{1}{\rho r}\frac{\partial}{\partial r}\left(-\rho r\overline{\frac{v'^3}{2}}\right)$
	D3	$\frac{1}{\rho r}\frac{\partial}{\partial r}\left(-\rho r\overline{\frac{u'^2v'}{2}}\right)$
	D4	$\frac{1}{\rho}\frac{\partial}{\partial x}\left(\mu\frac{\partial k}{\partial x}\right)$
	D5	$\frac{1}{\rho}\frac{\partial}{\partial x}\left(-\rho\overline{\frac{u'^3}{2}}\right)$
	D6	$\frac{1}{\rho}\frac{\partial}{\partial x}\left(-\rho\overline{\frac{u'v'^2}{2}}\right)$
	D7	$-\frac{\mu}{\rho}\overline{\frac{v'^2}{r^2}}$

Appendix A

REYNOLDS EQUATIONS

Assuming that U, V, and W are the velocity components in the directions of the cylindrical coordinates x, r, and θ, respectively, the conservation of mass equation could be expressed as

$$\frac{\partial \rho}{\partial t} + \frac{\partial (\rho U)}{\partial x} + \frac{1}{r}\frac{\partial (r\rho V)}{\partial r} + \frac{1}{r}\frac{\partial (\rho W)}{\partial \theta} = 0 \tag{A.1}$$

The conservation of momentum equations in the three coordinate directions, axial, radial, and tangential, are as itemized below:

1. Axial momentum equation:

$$\frac{\partial (\rho U)}{\partial t} + \frac{\partial (\rho U^2)}{\partial x} + \frac{1}{r}\frac{\partial (r\rho UV)}{\partial r} + \frac{1}{r}\frac{\partial (\rho UW)}{\partial \theta} = -\frac{\partial P}{\partial x} + \frac{\partial}{\partial x}\left[2\mu\frac{\partial U}{\partial x} - \frac{2}{3}\mu\sigma\right] + \frac{1}{r}\frac{\partial}{\partial r}\left[r\mu\left(\frac{\partial U}{\partial r} + \frac{\partial V}{\partial x}\right)\right] + \frac{1}{r}\frac{\partial}{\partial \theta}\left[\mu\left(\frac{\partial W}{\partial x} + \frac{1}{r}\frac{\partial U}{\partial \theta}\right)\right] \tag{A.2}$$

2. Radial momentum equation:

$$\frac{\partial (\rho V)}{\partial t} + \frac{\partial (\rho VU)}{\partial x} + \frac{1}{r}\frac{\partial (r\rho V^2)}{\partial r} + \frac{1}{r}\frac{\partial (\rho VW)}{\partial \theta} - \frac{\rho W^2}{r} = -\frac{\partial P}{\partial r} + \frac{\partial}{\partial x}\left[\mu\left(\frac{\partial U}{\partial r} + \frac{\partial V}{\partial x}\right)\right] + \frac{1}{r}\frac{\partial}{\partial r}\left[r\mu\left(2\frac{\partial V}{\partial r} - \frac{2}{3}\sigma\right)\right] + \frac{1}{r}\frac{\partial}{\partial \theta}\left[\mu\left(r\frac{\partial}{\partial x}\frac{V}{r} + \frac{1}{r}\frac{\partial V}{\partial \theta}\right)\right] - \frac{\mu}{r}\left[2\frac{\partial U}{\partial x} + \frac{2V}{r} - \frac{2}{3}\sigma\right] \tag{A.3}$$

3. Tangential momentum equation:

$$\frac{\partial (\rho W)}{\partial t} + \frac{\partial (\rho WU)}{\partial x} + \frac{1}{r}\frac{\partial (r\rho WV)}{\partial r} + \frac{1}{r}\frac{\partial (\rho W^2)}{\partial \theta} - \frac{\rho WV}{r} = -\frac{1}{r}\frac{\partial P}{\partial \theta} + \frac{\partial}{\partial x}\left[\mu\left(\frac{\partial W}{\partial x} + \frac{1}{r}\frac{\partial U}{\partial \theta}\right)\right] + \frac{1}{r^2}\frac{\partial}{\partial r}\left[r^2\mu\left(r\frac{\partial}{\partial r}\frac{W}{r} - \frac{1}{r}\frac{\partial V}{\partial \theta}\right)\right] + \frac{1}{r}\frac{\partial}{\partial \theta}\left[2\mu\left(\frac{1}{r}\frac{\partial W}{\partial \theta} + \frac{V}{r}\right) - \frac{2}{3}\sigma\right] \tag{A.4}$$

ϕ is defined to be

$$\frac{\partial U}{\partial x} + \frac{1}{r}\frac{\partial}{\partial r}(rV) + \frac{1}{r}\frac{\partial W}{\partial \theta}$$

Reynolds defined the instantaneous values of velocity, pressure, and density to be composed of a mean value and a fluctuating component as follows:

$$U = \overline{U} + u',$$

$$V = \overline{V} + v',$$

$$W = \overline{W} + w',$$

$$P = \overline{P} + p', \text{ and}$$

$$\rho = \overline{\rho} + \rho' \tag{A.5}$$

If these instantaneous values are substituted in the conservation of mass, the result is the time averaged continuity equation (time average is performed) as follows:

$$\frac{\partial \overline{\rho}}{\partial t} + \frac{\partial}{\partial x}\left(\overline{\rho}\overline{U} + \overline{\rho' u'}\right) + \frac{1}{r}\frac{\partial}{\partial r}\left(r\overline{\rho}\overline{V} + r\overline{\rho' v'}\right) + \frac{1}{r}\frac{\partial}{\partial \theta}\left(\overline{\rho}\overline{W} + \overline{\rho' w'}\right) = 0 \tag{A.6}$$

In a similar manner, the time averaged Reynolds equations for turbulent flow in the three coordinates may be obtained by substituting the instantaneous values into the momentum equations and time averaging. The following results are obtained:-

1. Time averaged axial Reynolds equation:

$$\frac{\partial}{\partial t}\left(\overline{\rho}\overline{U}\right) + \frac{1}{r}\frac{\partial}{\partial r}\left(r\overline{\rho}\overline{V}\ \overline{U}\right) + \frac{1}{r}\frac{\partial}{\partial \theta}\left(\overline{\rho}\overline{W}\ \overline{U}\right) + \frac{\partial}{\partial x}\left(\overline{\rho}\overline{U}\ \overline{U}\right) +$$

$$\left[\frac{1}{r}\frac{\partial}{\partial r}\left(r\overline{\rho v'u'}\right)+\frac{1}{r}\frac{\partial}{\partial\theta}\left(\overline{\rho u'u'}\right)+\frac{\partial}{\partial x}\left(\overline{\rho u'u'}\right)\right]+$$

$$\left[\frac{1}{r}\frac{\partial}{\partial r}\left(r\overline{U}\;\overline{\rho'v'}\right)+\frac{1}{r}\frac{\partial}{\partial\theta}\left(\overline{U}\;\overline{\rho'u'}\right)+\frac{\partial}{\partial x}\left(\overline{U}\;\overline{\rho'u'}\right)\right]+$$

$$\left[\frac{1}{r}\frac{\partial}{\partial r}\left(r\overline{V}\;\overline{\rho'u'}\right)+\frac{1}{r}\frac{\partial}{\partial\theta}\left(\overline{W}\;\overline{\rho'u'}\right)+\frac{\partial}{\partial x}\left(\overline{U}\;\overline{\rho'u'}\right)\right]+$$

$$\frac{\partial}{\partial t}\left(\overline{\rho'u'}\right)+\frac{1}{r}\frac{\partial}{\partial r}\left(r\overline{\rho'v'u'}\right)+\frac{1}{r}\frac{\partial}{\partial\theta}\left(\overline{\rho'u'u'}\right)+\frac{\partial}{\partial x}\left(\overline{\rho'u'u'}\right)=-\frac{\partial\overline{P}}{\partial x}+$$

$$\frac{1}{r}\frac{\partial}{\partial r}\left[r\mu\left(\frac{\partial\overline{U}}{\partial r}+\frac{\partial\overline{V}}{\partial x}\right)\right]+\frac{1}{r}\frac{\partial}{\partial\theta}\left[\mu\left(\frac{\partial\overline{W}}{\partial x}+\frac{1}{r}\frac{\partial\overline{U}}{\partial\theta}\right)\right]+\frac{\partial}{\partial x}\left[2\mu\frac{\partial\overline{U}}{\partial x}-\frac{2}{3}\mu\sigma\right] \tag{A.7}$$

2. Time averaged radial Reynolds equation:

$$\frac{\partial}{\partial t}\left(\overline{\rho}\overline{V}\right)+\frac{1}{r}\frac{\partial}{\partial r}\left(r\overline{\rho}\overline{V}\;\overline{V}\right)+\frac{1}{r}\frac{\partial}{\partial\theta}\left(\overline{\rho}\overline{W}\;\overline{V}\right)+\frac{\partial}{\partial x}\left(\overline{\rho}\overline{U}\;\overline{V}\right)-\frac{\overline{\rho}\overline{W}\;\overline{W}}{r}+$$

$$\left[\frac{1}{r}\frac{\partial}{\partial r}\left(r\overline{\rho v'v'}\right)+\frac{1}{r}\frac{\partial}{\partial\theta}\left(\overline{\rho u'v'}\right)+\frac{\partial}{\partial x}\left(\overline{\rho u'v'}\right)-\frac{\overline{\rho u'u'}}{r}\right]+$$

$$\left[\frac{1}{r}\frac{\partial}{\partial r}\left(r\overline{V}\;\overline{\rho'v'}\right)+\frac{1}{r}\frac{\partial}{\partial\theta}\left(\overline{V}\;\overline{\rho'u'}\right)+\frac{\partial}{\partial x}\left(\overline{V}\;\overline{\rho'u'}\right)-\frac{\overline{\rho'u'}\;\overline{W}}{r}\right]+$$

$$\left[\frac{1}{r}\frac{\partial}{\partial r}\left(r\overline{V}\;\overline{\rho'v'}\right)+\frac{1}{r}\frac{\partial}{\partial\theta}\left(\overline{W}\;\overline{\rho'v'}\right)+\frac{\partial}{\partial x}\left(\overline{U}\;\overline{\rho'v'}\right)-\frac{\overline{\rho'u'}\;\overline{W}}{r}\right]+$$

$$\frac{\partial}{\partial t}\left(\overline{\rho'v'}\right)+\frac{1}{r}\frac{\partial}{\partial r}\left(r\overline{\rho'v'v'}\right)+\frac{1}{r}\frac{\partial}{\partial\theta}\left(\overline{\rho'u'v'}\right)+\frac{\partial}{\partial x}\left(\overline{\rho'u'v'}\right)-\frac{\overline{\rho'u'u'}}{r}=-\frac{\partial\overline{P}}{\partial r}+$$

$$\frac{1}{r}\frac{\partial}{\partial r}\left[r\mu\left(2\frac{\partial\overline{V}}{\partial r}-\frac{2}{3}\sigma\right)\right]+\frac{1}{r}\frac{\partial}{\partial\theta}\left[\mu\left(r\frac{\partial}{\partial x}\frac{\overline{V}}{r}+\frac{1}{r}\frac{\partial\overline{V}}{\partial\theta}\right)\right]-\frac{\mu}{r}\left[2\frac{\partial\overline{U}}{\partial x}+\frac{2\overline{V}}{r}-\frac{2}{3}\sigma\right]+$$

$$\frac{\partial}{\partial x}\left[\mu\left(\frac{\partial\overline{U}}{\partial r}+\frac{\partial\overline{V}}{\partial x}\right)\right] \tag{A.8}$$

3. Time averaged tangential Reynolds equation:

$$\frac{\partial}{\partial t}\left(\overline{\rho}\overline{W}\right)+\frac{1}{r}\frac{\partial}{\partial r}\left(r\overline{\rho}\overline{V}\;\overline{W}\right)+\frac{1}{r}\frac{\partial}{\partial\theta}\left(\overline{\rho}\overline{W}\;\overline{W}\right)+\frac{\partial}{\partial x}\left(\overline{\rho}\overline{U}\;\overline{W}\right)+\frac{\overline{\rho}\overline{V}\;\overline{W}}{r}+$$

$$\left[\frac{1}{r}\frac{\partial}{\partial r}\left(r\overline{\rho v'w'}\right)+\frac{1}{r}\frac{\partial}{\partial\theta}\left(\overline{\rho w'w'}\right)-\frac{\partial}{\partial x}\left(\overline{\rho u'w'}\right)+\frac{\overline{\rho v'w'}}{r}\right]+$$

$$\left[\frac{1}{r}\frac{\partial}{\partial r}\left(r\overline{W}\;\overline{\rho'v'}\right)+\frac{1}{r}\frac{\partial}{\partial\theta}\left(\overline{W}\;\overline{\rho'w'}\right)+\frac{\partial}{\partial x}\left(\overline{W}\;\overline{\rho'u'}\right)+\frac{\overline{\rho'v'}\;\overline{W}}{r}\right]+$$

$$\left[\frac{1}{r}\frac{\partial}{\partial r}\left(r\overline{V}\;\overline{\rho'w'}\right)+\frac{1}{r}\frac{\partial}{\partial\theta}\left(\overline{W}\;\overline{\rho'w'}\right)+\frac{\partial}{\partial x}\left(\overline{U}\;\overline{\rho'w'}\right)+\frac{\overline{\rho'w'}\;\overline{V}}{r}\right]+$$

$$\frac{\partial}{\partial t}\left(\overline{\rho'w'}\right)+\frac{1}{r}\frac{\partial}{\partial r}\left(r\overline{\rho'w'w'}\right)+\frac{1}{r}\frac{\partial}{\partial\theta}\left(\overline{\rho'w'w'}\right)+\frac{\partial}{\partial x}\left(\overline{\rho'u'w'}\right)-$$

$$\frac{\overline{\rho'v'w'}}{r}=-\frac{1}{r}\frac{\partial\overline{P}}{\partial\theta}+\frac{1}{r^2}\frac{\partial}{\partial r}\left[r^2\mu\left(r\frac{\partial}{\partial r}\frac{\overline{W}}{r}-\frac{1}{r}\frac{\partial\overline{V}}{\partial\theta}\right)\right]+\frac{1}{r}\frac{\partial}{\partial\theta}\left[2\mu\left(\frac{1}{r}\frac{\partial\overline{W}}{\partial\theta}+\frac{\overline{V}}{r}\right)-\frac{2}{3}\rho\right]+$$

$$\frac{\partial}{\partial x}\left[\mu\left(\frac{\partial\overline{W}}{\partial x}+\frac{1}{r}\frac{\partial\overline{U}}{\partial\theta}\right)\right] \qquad (A.9)$$

The Reynolds equations in tensor form could be written as:

$$\frac{\partial}{\partial t}\left(\overline{\rho}\overline{U_i}\right)+\frac{\partial}{\partial t}\left(\overline{\rho'u_i'}\right)+\frac{\partial}{\partial x_j}\left(\overline{\rho}\;\overline{U_i}\;\overline{U_j}\right)+\frac{\partial}{\partial x_j}\left(\overline{U_i}\;\overline{\rho'u'}\right)+\frac{\partial}{\partial x_j}\left(\overline{U_j}\;\overline{\rho'u_i'}\right)+\frac{\partial}{\partial x_j}\left(\overline{\rho}\;\overline{u_i'u_j'}\right)+$$

$$\frac{\partial}{\partial x_j}\left(\overline{\rho'u_i'u_j'}\right)=-\frac{\partial\overline{P}}{\partial x_i}+\frac{\partial}{\partial x_j}\left[\mu\left(\frac{\partial\overline{U_i}}{\partial x_j}+\frac{\partial\overline{U_j}}{\partial x_i}-\frac{2}{3}\delta_{ij}\frac{\partial\overline{U_k}}{\partial x_k}\right)\right] \qquad (A.10)$$

For constant density flow (or neglecting the fluctuations in the density), the above equation reduces to the following form:-

$$\frac{\partial}{\partial t}\left(\overline{\rho}\overline{U_i}\right)+\frac{\partial}{\partial x_j}\left(\overline{\rho}\;\overline{U_i}\;\overline{U_j}\right)+\frac{\partial}{\partial x_j}\left(\overline{\rho}\;\overline{u_i'u_j'}\right)=-\frac{\partial\overline{P}}{\partial x_i}+\frac{\partial}{\partial x_j}\left[\mu\frac{\partial\overline{U_i}}{\partial x_j}\right]+\frac{\partial\overline{U_j}}{\partial x_i}\frac{\partial\mu}{\partial x_j} \qquad (A.11)$$

if cartesian coordinates were used instead of cylindrical coordinates, these coordinate transformation equations could be utilized:

$$x=x,\;y=r\;and\;z=r\theta$$

and the equations in rectangular coordinates could be evaluated.

Appendix B

TURBULENCE ENERGY EQUATION

The turbulence energy equation could be derived by multiplying the *ith* Reynolds equation by u_i' ($i = 1, 2$ *and* 3) and then summing all the equations. The new equation in tensor form is as follows:-

$$\overline{\rho' u_i'}\frac{\partial \overline{U}_i}{\partial t} + \frac{\partial}{\partial t}(\overline{\rho} k) + \frac{\partial}{\partial t}\left(\overline{\rho' k}\right) + \frac{\partial}{\partial x_j}\left(\overline{\rho}\,\overline{U}_j k\right) + \frac{\partial}{\partial x_j}\left(\overline{U}_j\,\overline{\rho' k}\right) +$$

$$\left[\frac{\partial}{\partial x_j}\left(\overline{\rho u_j' k}\right) + \frac{\partial}{\partial x_j}\left(\overline{\rho' u_j' k}\right) + \overline{\rho}\,\overline{u_i' u_j'}\frac{\partial \overline{U}_i}{\partial x_j} + \overline{\rho' u_i'}\,\overline{U}_j\frac{\partial \overline{U}_i}{\partial x_j}\right] + \overline{\rho' u_i' u_j'}\frac{\partial \overline{U}_i}{\partial x_j} = -\frac{\partial}{\partial x_i}\left(\overline{u_i' \rho'}\right) + \overline{\rho'\frac{\partial u_i'}{\partial x_i}} +$$

$$\frac{\partial}{\partial x_j}\left[\mu\frac{\partial}{\partial x_j}(k)\right] - \mu\overline{\left[\frac{\partial u_i'}{\partial x_j}\right]^2} + \overline{u_i'\frac{\partial u_j'}{\partial x_i}}\frac{\partial \mu}{\partial x_j} + \frac{1}{3}\mu\overline{u_i'\frac{\partial}{\partial x_i}\left[\frac{\partial u_k'}{\partial x_k}\right]} - \frac{2}{3}\overline{u_j'\frac{\partial \mu}{\partial x_j}\left[\frac{\partial u_k'}{\partial x_k}\right]} \quad \text{(B.1)}$$

For constant density flow (or neglecting the fluctuations in the density), the above equation becomes:

$$\frac{\partial}{\partial t}(\overline{\rho} k) + \frac{\partial}{\partial x_j}\left(\overline{\rho}\,\overline{U}_j k\right) + \frac{\partial}{\partial x_j}\left(\overline{\rho u_j' k}\right) + \overline{\rho}\,\overline{u_i' u_j'}\frac{\partial \overline{U}_i}{\partial x_j} = -\frac{\partial}{\partial x_i}\left(\overline{u_i' \rho'}\right) + \frac{\partial}{\partial x_j}\left[\mu\frac{\partial}{\partial x_j}(k)\right] -$$

$$\mu\overline{\left[\frac{\partial u_i'}{\partial x_j}\right]^2} + \overline{u_i'\frac{\partial u_j'}{\partial x_i}}\frac{\partial \mu}{\partial x_j} \quad \text{(B.2)}$$

This equation in cylindrical coordinates (for steady, axisymmetric, and constant density flow) could be written as

$$\overline{U}\frac{\partial k}{\partial x} + \overline{V}\frac{\partial k}{\partial r} = \frac{1}{\rho}\frac{\partial}{\partial x}\left[\mu\frac{\partial k}{\partial x} - \rho\frac{\overline{u'v'v'}}{2} - \rho\frac{\overline{u'w'w'}}{2} - \rho\frac{\overline{u'u'u'}}{2} - \overline{u'p'}\right] +$$

$$\frac{1}{\rho r}\frac{\partial}{\partial r}\left[\mu r\frac{\partial k}{\partial r} - \rho r\frac{\overline{v'v'v'}}{2} - \rho r\frac{\overline{v'w'w'}}{2} - \rho r\frac{\overline{u'u'v'}}{2} - r\overline{v'p'}\right] - \left[\frac{2}{\rho}\mu\frac{\overline{v'v'}}{r^2} - \frac{\mu}{\rho}\frac{\overline{w'w'}}{r^2}\right] -$$

$$\left[\overline{v'v'}\frac{\partial \overline{V}}{\partial r} + \overline{u'v'}\frac{\partial \overline{U}}{\partial r} + \overline{u'v'}\frac{\partial \overline{V}}{\partial x} + \overline{u'u'}\frac{\partial \overline{U}}{\partial x} + \overline{w'w'}\frac{\overline{V}}{r}\right] -$$

$$\frac{\mu}{\rho}\left[\overline{\left(\frac{\partial v'}{\partial r}\right)^2} + \overline{\left(\frac{\partial w'}{\partial r}\right)^2} + \overline{\left(\frac{\partial u'}{\partial r}\right)^2} + \overline{\left(\frac{\partial v'}{\partial x}\right)^2} + \overline{\left(\frac{\partial w'}{\partial x}\right)^2} + \overline{\left(\frac{\partial u'}{\partial x}\right)^2}\right] \quad \text{(B.3)}$$

Appendix C

COMPONENTS OF TKE TERMS

Components of Production Terms

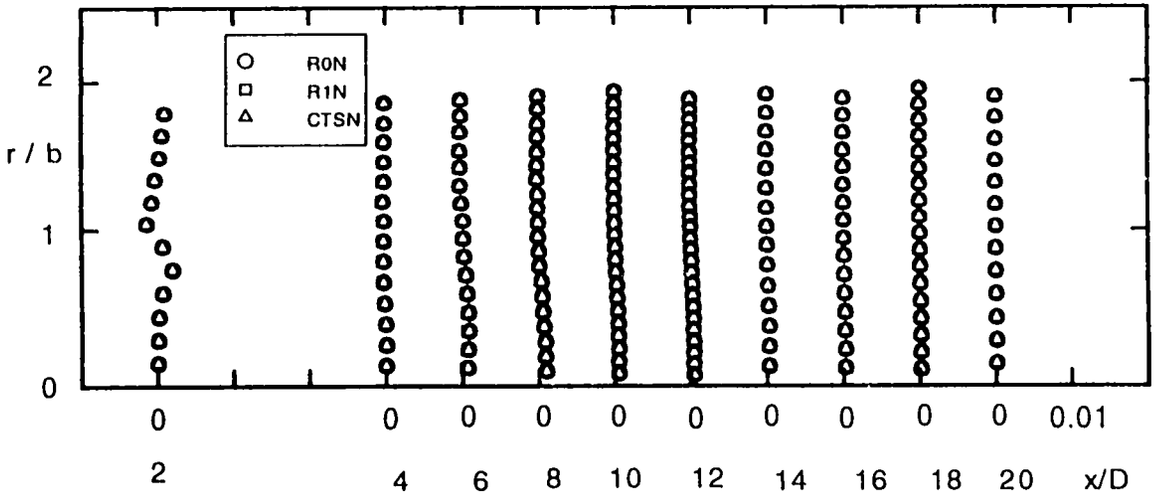

Figure C.1: Evolution of first component of normalized total production, P1

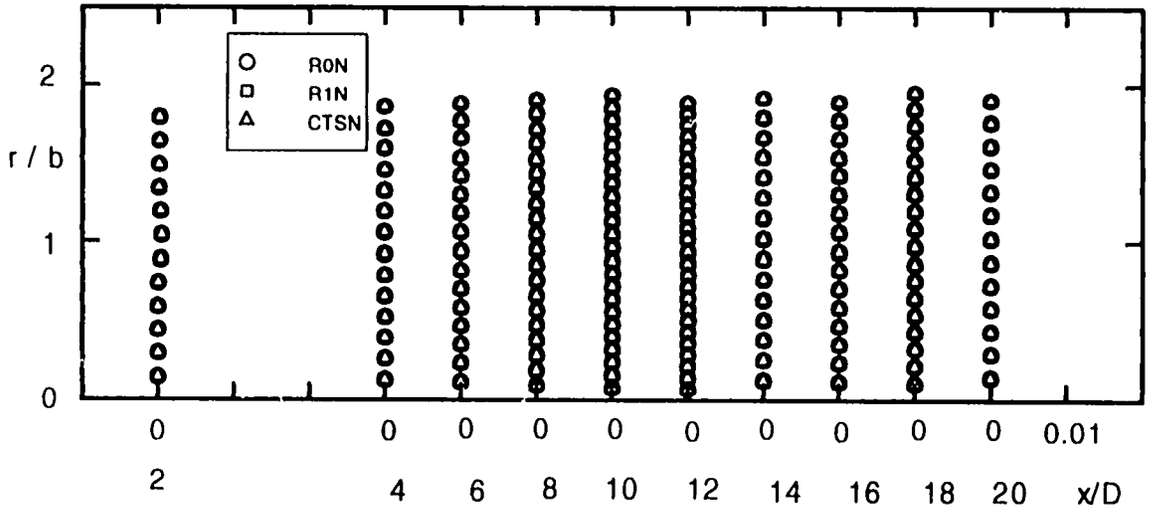

Figure C.2: Evolution of second component of normalized total production, P2

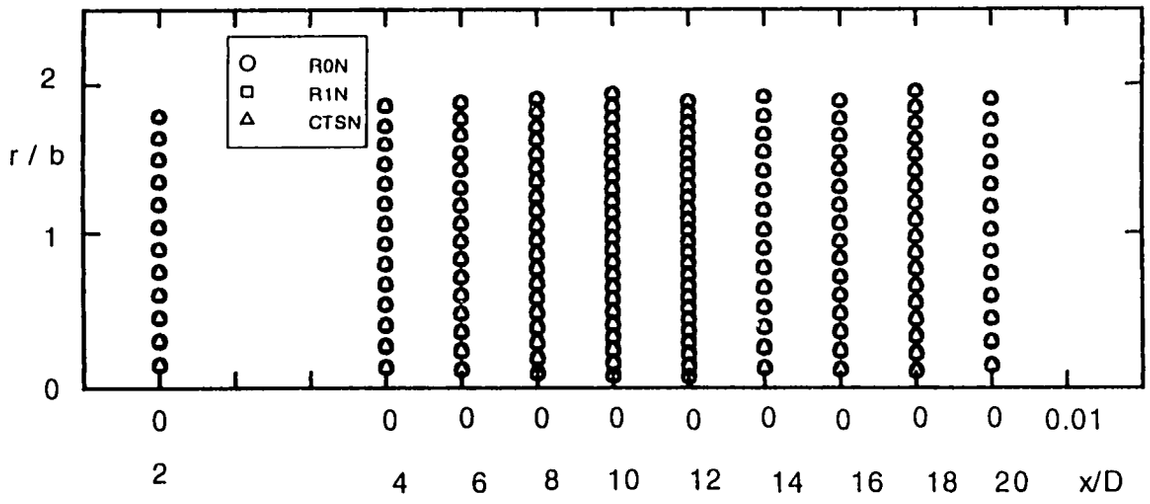

Figure C.3: Evolution of third component of normalized total production, P3

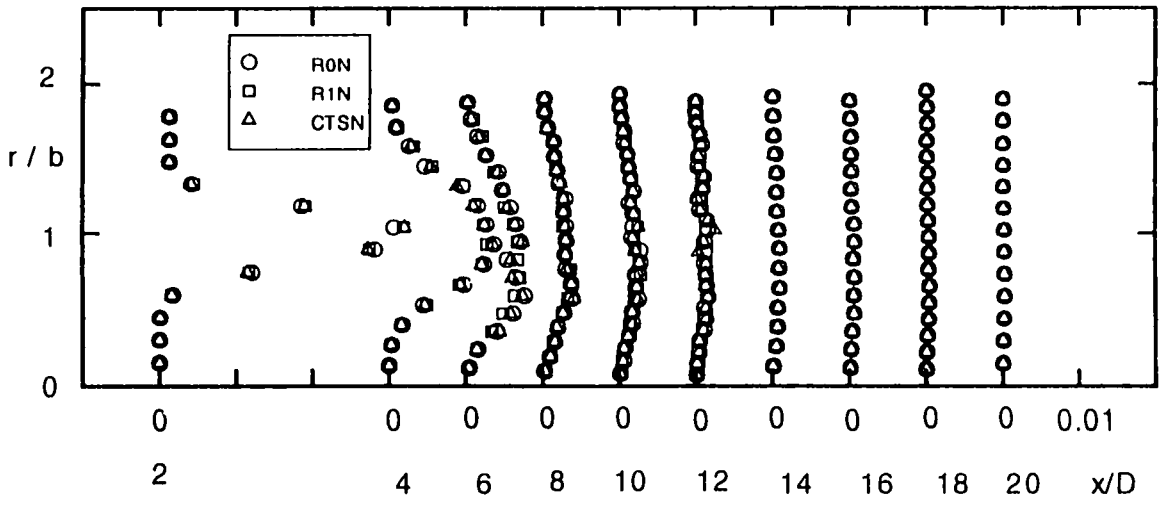

Figure C.4: Evolution of fourth component of normalized total production, P4

Components of Convection Terms

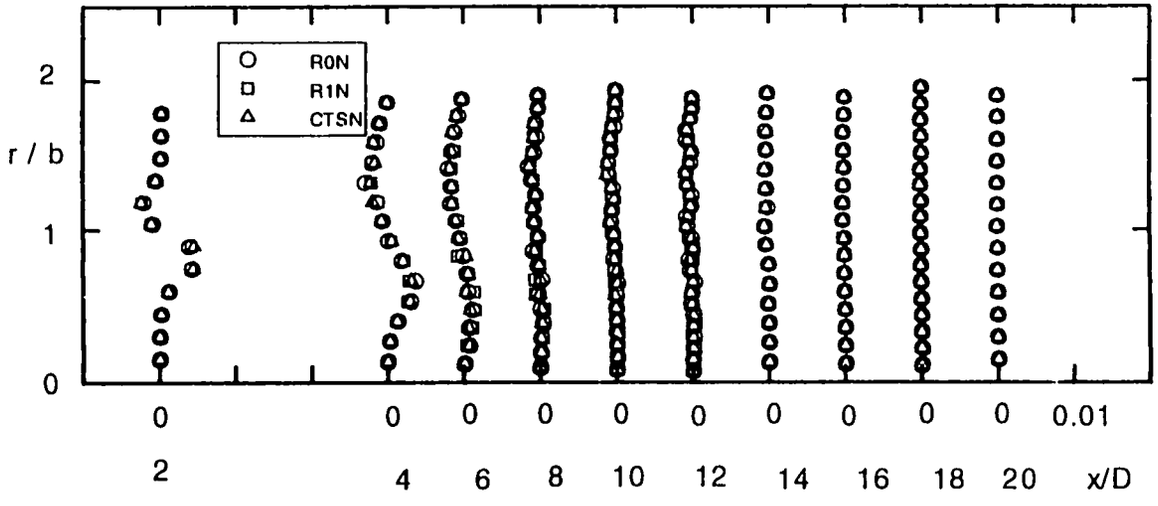

Figure C.5: Evolution of first component of normalized total convection, C1

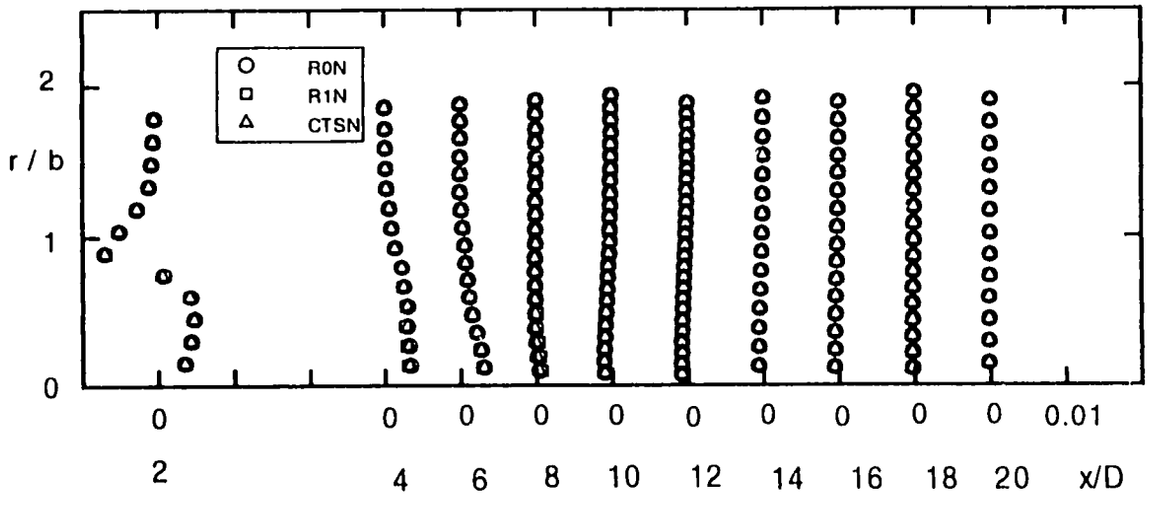

Figure C.6: Evolution of second component of normalized total convection, C2

Components of Diffusion Terms

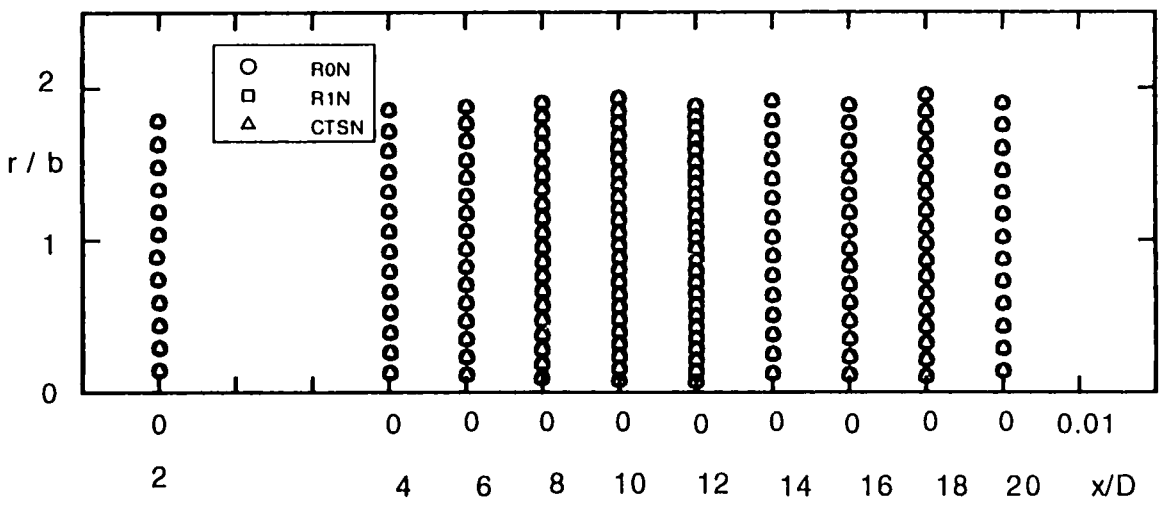

Figure C.7: Evolution of first component of normalized total diffusion, D1

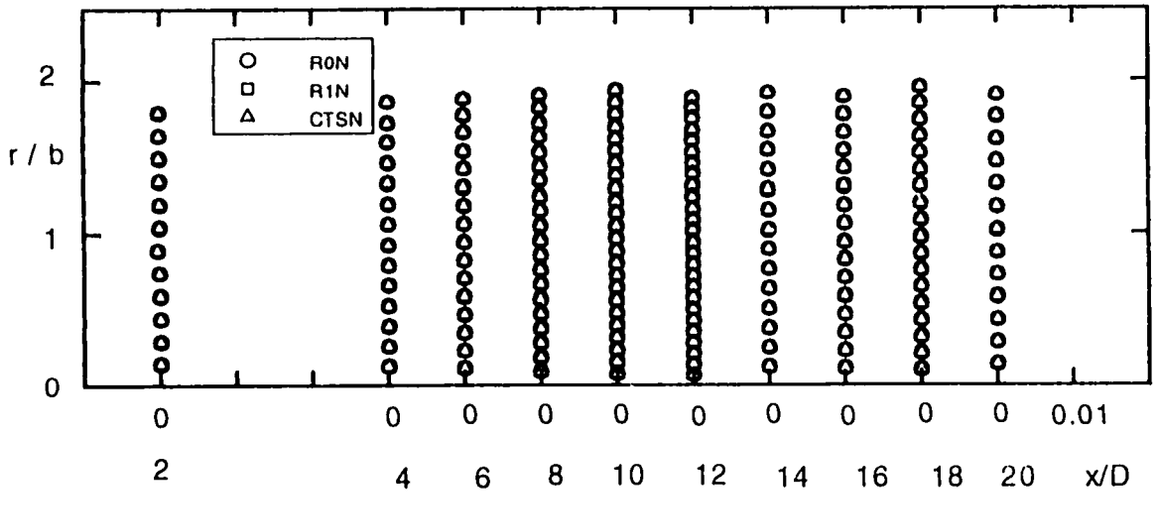

Figure C.8: Evolution of second component of normalized total diffusion, D2

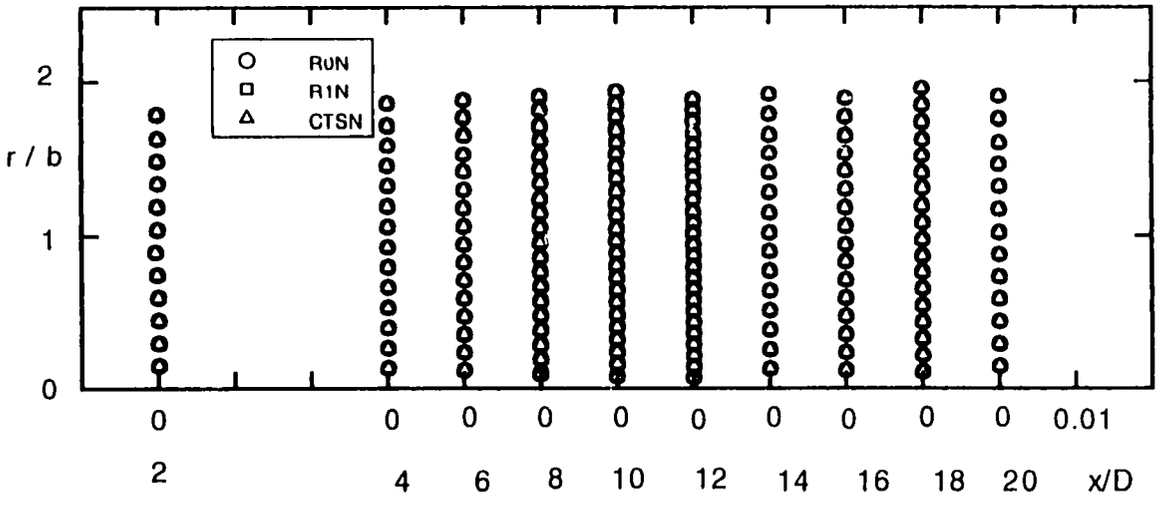

Figure C.9: Evolution of third component of normalized total diffusion, D3

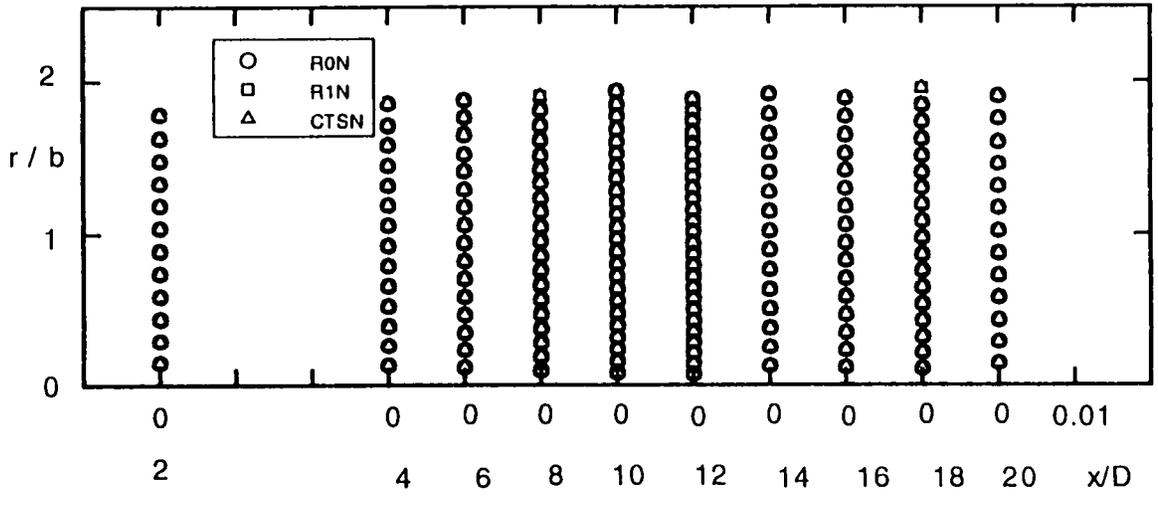

Figure C.10: Evolution of fourth component of normalized total diffusion, D4

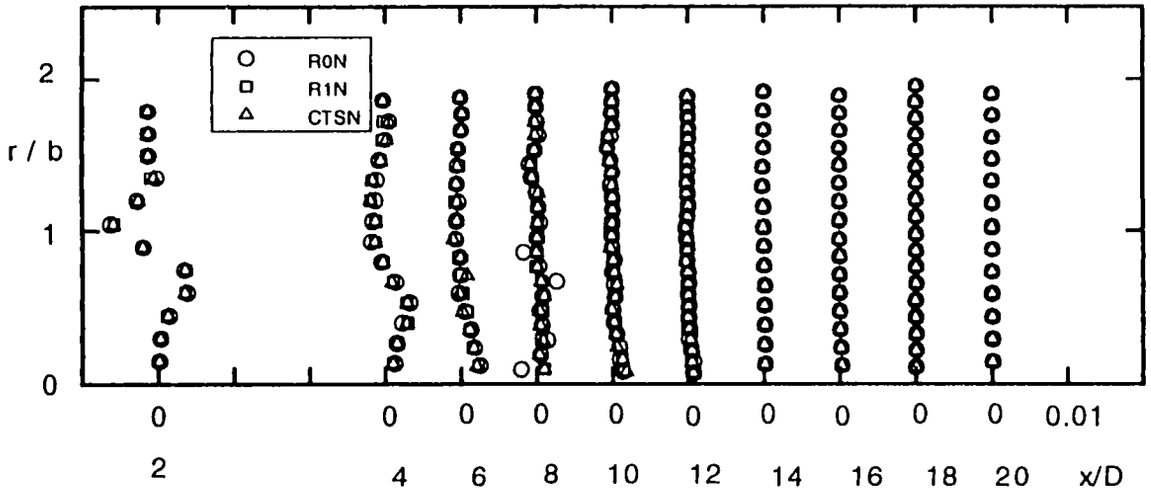

Figure C.11: Evolution of fifth component of normalized total diffusion, D5

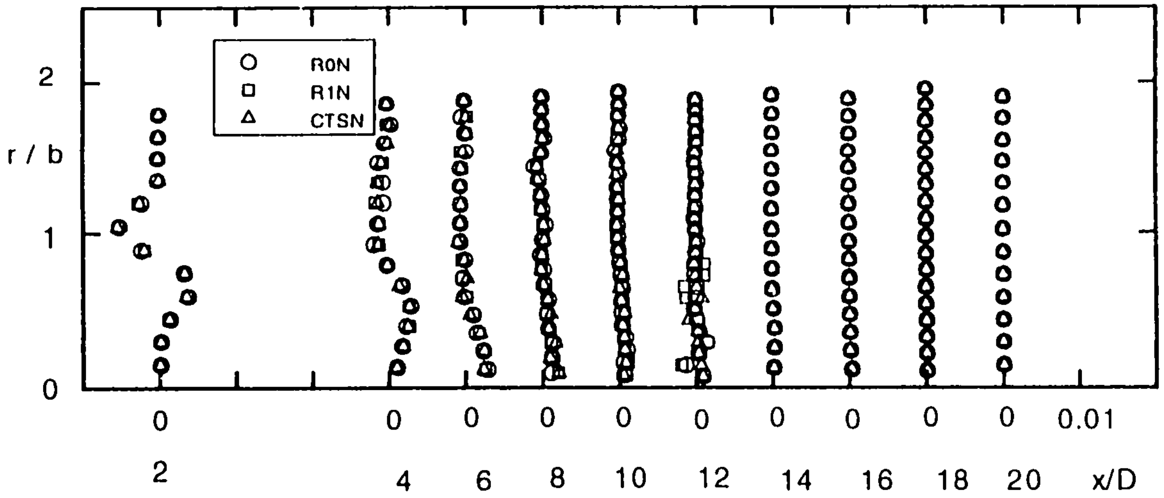

Figure C.12: Evolution of sixth component of normalized total diffusion, D6

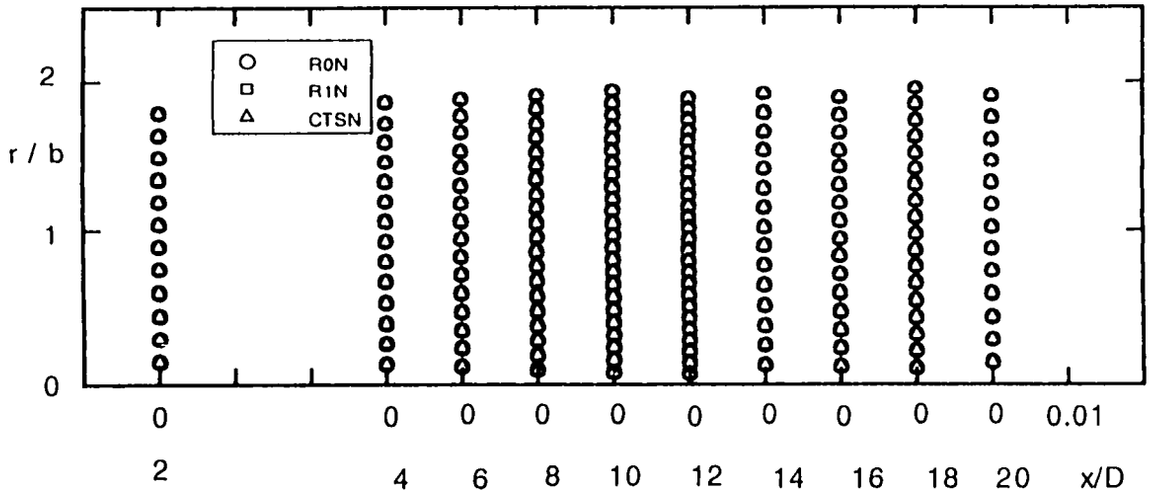

Figure C.13: Evolution of seventh component of normalized total diffusion, D7

Nomenclature

D	Free jet nozzel diameter.
R	Nozzel exit radius.
r	Radial measurement coordinate.
b	Jet half width
U	Mean velocity.
$\overline{U}$	Mean axial velocity.
u'	Fluctuating axial velocity.
v'	Fluctuating radial velocity.
V	radial velocity.
$\overline{V}$	mean velocity in r direction.
$\overline{u'v'}$	Reynold's shear stress.
x	Axial measurment coordinate.
CT	Normalized total convection term.
C_i, i=1,2...	Component parts of normalized total convection term.
PT	Normalized total production term.
P_i, i=1,2..	Component parts of normalized total production term.
VDT	Normalized total viscous dissipation term.
k	$\frac{1}{2}(\overline{u'^2} + \overline{v'^2} + \overline{w'^2})$, turbulent kinetic energy.
NIF	Normalized non-isotropic factor.

DT	Normalized total diffusion term.
D_i, i=1,2,..	Component parts of normalized total diffusion term.
RON	Particle Average.
RIN	Time between two data average.
CTSN	Periodic Sampling.
f_p	Frequency of valid particle arrival.
f_s	Sampling frequency.
$\omega_j = 1$	weighting value for particle average scheme.
$\omega_j = T_{bd}$	weighting value for T_{bd} average.
$\omega_j = \frac{1}{f_s}$	weighting value for constant periodic sampling.
RMS	Root mean square

Subscripts .

cl	Centerline of jet.
o	Jet exit condition.

Supercripts / .

-	Time mean value.
'	Fluctuating component.

Bibliography

[1] Corrsin, S. and Uberoi, M. S., "Spectrums and Diffusion in a Round Turbulent Jet", 1949, NASA Reoprt 1040.

[2] Kolpin, M. A., "The Flow in the Mixing Region of a Jet", Journal of Fluid Mechanics, Vol. 18, 1964, pp. 529-548.

[3] Davies, P. O. A. L., Fisner, M. J. and Barrett, M. J., "Turbulence in the Mixing Region of a Round Jet", Journal of Fluid Mechanics, Vol. 15, 1963, pp. 337-367.

[4] Wygnanski, I. and Fiedler, H. ,"Some Measurements in Self-preserving Jet", Journal of Fluid Mechanics, Vol. 38, 1969, pp. 577-612.

[5] Rodi, W., "A New Method of Analysing Hot-wire Signals in Highly Turbulent Flow, and Its Evaluation in a Round Jet", DISA Information, 1975 No. 17.

[6] Bradshaw, P., Ferris, D. H. and Johnson, R. F., "Turbulence in the Noise Producing Region of a Circular Jet" . Journal of Fluid Mechanics, 1964 Vol.19, pp. 591-624.

[7] Corrsin, S., "Investigation of Flow in an Axially Symmetrical Heated Jet of Air". 1943 NACA Wartime Report W94.

[8] Sami, S., Carmody T., and Rouse H., "Jet Diffusion in the Region of Flow Establishment.", Journal of Fluid Mechanics, Vol. 27, 1967, pp. 231-252.

[9] Mckillop, B. E., "Turbulence Measurements in A Complex Flow Field Using A Crossed Hot-Wire.", M.Sc. Thsis, Oklahoma State University, 1981.

[10] N. Ninomiya and N. Kasagi, "Measurement of the Reynolds Stress Budgets in an Axisymmetric Free Jet with the Aid of Three-Dimensional Particle Tracking Velocimetry.", Nine Symposium on " Turbulent Shear Flows" , Kyoto, Japan, August 16-18, 1993, pp. 1-6.

[11] Goldstein, S., "A Note on the Measurement of Total Head and Static Pressure in Turbulent Stream." Preoceedings of Royal Society, London, A155, 1936, pp. 570-575.

[12] Hinze, J. O. Turbulence, McGraw-Hill, New york, 1957.

[13] Gettelman, C. C. and Krause, L. N. "Considerations Entering into the Selection of Probes for Pressure Measurement in Jet Engines." ISA Proceedings, Vol. 7, 1952, pp. 134-136.

[14] Bradshaw, P. An Introduction to Turbulence and its Measurements. Pergamon Pres, New York, 1971.

[15] Pai, Shih-i.," Viscous Flow Theory, II Turbulent Flow." D. Van Nostrand Company, Inc., Princeton, N. J., 1957.

[16] Jones, B. G. "Modern Turbulence Measuring and Analyzing Techniques. " Advanced Heat Transfer Lecture Series, University of Illinois, Urbana, Illinois, April 1967.

[17] Yeh, Y. and Cummins, H. Z. "Localized Fluid Flow Measurements with a He-Ne Laser Spectrometer." Applied Physics Letters, Vol. 4, No. 10, May 1964, pp. 176-178.

[18] Lennert, A. E., Brayton, D. B., Crosswy, P. L. "Summary Report of the Development of a Laser Velocimeter to be used in AEDC Wind Tunnels. " AEDC-TR-70-101, (AD871321), July 1970.

[19] Stevenson, W. H., and Thompson, H. D., editors. "The Use of the Laser Doppler Velocimeter for Flow Measurements. Project SQUID Report, Jet

Propulsion center, Purdue University, West Lafayette, Indiana, November 1972.

[20] McLaughlin, D. and Tiederman, W. G., Co-directions. "Theory and Application of the Laser Doppler Anemometer." Oklahoma State University, Laser Doppler Anemometer Workshop, Oklahoma State University, Stillwater, Oklahoma, June 1973.

[21] Stevenson, W. H. and Thompson, H. D., editors. Proceedings of the second International Workshop on Laser Velocimetery, Engineering Experiment Station Bulletin No. 144, Purdue University, West Lafayette, Indiana, March 1974.

[22] Rudd, M. J. "A Self Aligning Laser Doppler Velocimeter." Optical Instruments and Techniques, 1969, pp. 158-166.

[23] George, W. K. and Lumley, J. L. "The Laser-Doppler Veloctimeter and its Application to the Measurement of Turbulence." Journal of Fluid Mechanics, Vol. 60, Part 2, 1973, pp. 321-362.

[24] Brayton, D. B., Kalb, H. T., and Crosswy, F. L. "A Two-Component Dual-scatter Laser Doppler Velocimeter with Frequency Burst Signal Readout." Applied Optics, Vol. 12, No. 6, June 1973, pp. 1145-1156.

[25] Asher, J. A. "Laser Doppler Velocimeter System Development and Testing." General Electric Technical Information Series Report No. 72CRD295, Corporate Research & Development Distribution, Schenectady, N. Y., October 1972.

[26] Meak, C. C. and Jones, B. G. "Studies of the Behavior of Heavy Particles in a Turbulence Fluid Flow." Journal of Atmospheric Sciences, Vol. 30, No. 2, March 1973, pp. 239-244.

[27] Berman, N. S. "Particle-Fluid Interaction Corrections for Flow Measurements with a Laser Doppler Flowmeter." NASA-CR-124254, 1972.

[28] Khosla, P. K. and Lederman, S. "Motion of a Spherical Particle in a Turbulent Flow." Contract Report PIBAL 73-22 (AD779541) under Contract DAHC04-00-C-007, Polytechinic Institute of New York, Farmingale, New York, November 1973.

[29] Yanta, W. J. "Turbulence Measurements with a Laser Doppler Velocimeter." Naval Ordnance Laboratory Report NOL TR- 73-94, May 1973.

[30] Longan, S. E. "A Laser Velocitmeter for Reynolds Stress and Other Turbulence Measurements." AIAA Journal Vol. 10, No. 7, July 1972, pp. 933-935

[31] Farmer, W. M. and Hornkohl, J. O. "Two - Component, Self-Aligning Laser Vector Velocimeter." Applied Optics, Vol. 12, No. 11, November 1973, pp. 123- 140.

[32] McLaughlin, D., and Tiederman, W., "Biasing Correction for Individual Realization of Laser Anemometer Measurements in Turbulent Flows." The Physics of Fluids, Vol. 16, No.12, December 1973, pp. 2082.

[33] Durao, D. and Whitelaw, J. H., "The Influence of Sampling Procedures on Velocity Bias in Turbulent Flows." Proceedings of the LDV Symposium, Copenhagen, 1975, pp. 138.

[34] Quigley, M. and Tiederman, W., "Experimental Evaluation of Sampling Bias in Individual Realization Laser Anemometry." AIAA Journal, Vol. 15, No. 2, February 1977, pp. 226.

[35] Bogard, D. and Tiederman, W., "Experimental Evaluation of Sampling Bias in Naturally Seeded Flows." Laser Velocimetry and Particle Sizing, Hemisphere Publishing Corporation, 1979, pp. 86.

[36] Barnett, D. O., and Bentley, H. T., "Statistical Bias of Individual Realization Laser Velocimeters." Proceedings of the Second International Workshop on Laser Velocimetry, Purdue University, March 1974.

[37] Hoesel, W. and Rodi, W. "New Biasing Elimination Method for Laser Doppler Velocimeter Counter Processing". Review of Scientific Instruments, Vol. 48, No. 7, 1977, pp. 910.

[38] Giel, T. and Barnett, D., "Analytical and Experimental Study of Statistical Bias in Laser Velocimetery." Laser Velocimetery and Particle Sizing, Hemisphere Puplishing Corporation, 1979, pp. 86.

[39] Johnson, D. A.; Bachalo, W. D.; and Moddaress, D., "Laser Velocimetery Applied to Transonic and Supersonic Aerodynamics." AGARD Conference Proceedings No. 193 on Applications of Non-Intrusive Instrumentation in Fluid Flow Research, 1976.

[40] Dimstakis, P. E.; Collins, D. J., and Lang, D. B., "Laser Doppler Velocity Measurements in Subsonic, Transonic and Supersonic Turbulent Boundary Layers." Laser Velocimetry and Particle Sizing, Hemisphere Puplishing Corporation, 1979, pp. 208.

[41] Craig, R. R., Nejad, A. S., "Velocity biasing of Two-Component LDV Data in Low-Turbulence Flows" AIAA Journal, 1985 Vol. 23, No 6, pp. 973-974.

[42] Simpson, R. L., and Chew, Y.T., "Measurements in Steady and Unsteady Separated Turbulent Boundary Layers." Laser Velocimetery and Particle

Sizing, et. H. D. Thompson and W. H. Stevenson. Hemisphere Puplishing. 1979.

[43] Roesler, T. Stevenson, W. H. and Thompson, H. D., "Investigation of Bias Errors in Laser Doppler Velocimeter Measurements." AFWAL-TR-80-2108. Dec 1980.

[44] Stevenson W. H., Thompson H. D. and Luchik, T. S., "Laser Velocimeter Measurements and Analysis in Turbulent Flows with Combustion." AFWAL-TR-82-2076. Part I, July 1983.

[45] Craig, R. R., Nejad, A. S., Hahn, E. Y., and Schwartzkopf, K. G., "A General Approach for obtaining Unbiased LDV Data in Highly Turbulent Non-Reacting and Reacting Flows" AIAA Paper No. 84-0366, 1984.

[46] Nejad, A. S., Favaloro, S. C., Vanka, S. P., Samimy, M. and Langenfled, C., "Application of Laser Velocimetry for Characterisation of Confined Swirling Flow" 33rd ASME International Gas Turbine and Aeroeengine Conference and Exposition, Amesterdam, 88-GT-159, 1988.

[47] Nejad, A. S. and Davis, D. L., "Velocity Bias in Two-Individual Realization Laser Doppler Velocimetry" Proceeding of Laser and Electro Optics, 1986.

[48] Snyder, P. K. Orloff and M. S. Reinath, " Redaction of Flow Measurement Uncertainties in Laser Velocimeters With Non-orthogonal Channels," AIAA Journal, Vol. 22, No. 8, pp. 1115-1123.

[49] Stevenson, W. H., and H. D. Thompson,"Direct Measurement of Laser Velocimeter Bias Errors in a Turbulent Flow" AIAA Journal, 20, No. 12, Dec. 1982 , pp. 1720-1723.

[50] Erdmann, J. C., and C. Tropea,"Statistical Bias in Laser Anemometry" SFB 80/ET/198, Univ. Karlsruhe, August 1981.

[51] Adams, E. W. and Eaton, J. K., "An LDV study of the Backward-Facing Step Flow, Including the Effects of Velocity Bias" Internotional Symposium on Laser Anemometry, Miami Beach, 1985.

[52] Buchhave, P., "Biasing Errors in Individual Particle Measurements with the LDV-Counter Singal Processor" Proc of the LDV Symposium, Copenhagen, 1975, pp 258-279.

[53] Meyers, J. F. and Wilkinson, S. P., "A Comparison of Turbulence Intensity Measurements Using a Laser Velocimeter and Hot Wire in a Low Speed Jet Flow" International Symposium on Application of Laser Doppler Anemometry to Fluid Mechanics, Lisbon, 1982.

[54] George W. K. ," The Self-preservation of turbulent flows and its relation to initial condtions case". AIAA Journal. 29. No. 15. Dec. 1989.

[55] Hussain J. Hussain. Steven P. Copp and William K. George.. "Velocity Measurements in a High-Reynolds-Numbers. Momentum-Conserving. Axisymmetric. Turbelent Jet." Journal of Fluid Mechanics. 1994. pp. 31-74

[56] Chen T. H.. Lightman A. J.. Yaney P. P. and Schmoll W. J.. " Simultaneous Velocity and Concentration Measurements of turbulant Jet Flows. " AIAA Journal. Vol.16. 1989. pp.52-66.

[57] Amano R. S. and Chal J. C.. " A closure Model of Diffusion Transport of the Reynolds-Stress equations and Its Application to a Turbulent Step Flow." Journal of Fluid Mechanics. Vol. 118. 1982. pp. 178-199.

[58] Gould. R.D.. Stevenson. W.H. and Thompson. H.D.. "Investigation of Turbulent Transport in an Axisymmetric Sudden Expansion ." AIAA Journal. Vol. 28. 1990. pp. 276-283

[59] Bayazitoglu. Y. and Peterson. J.." Measurements in Axisymmetric Jets Using LDV. "Third International Symposium on Laser Anemometry.Boston. 1987.

[60] Chandrasuda. C. and Bradshaw. P.. "Turbulence Structure of a Reattaching Mixing Layer." Journal of Fluid Mechanics. Vol. 110. 1981. pp. 171-194.

[61] Driver, D. M., and Seegmiller, H. L., "Features of a Reattaching Turbulent Shear Layer in Divergent Channel Flow" AIAA Journal, Vol.23, No 2, 1985, pp 163-171.

[62] Lapidus, L. , and Pinder, G. F. , "Numerical Solution of Partial Diffrential Equations in Science and Engineering", John Wiley and Sons, New York, (1982).